Department of Aeronautics and Astronautics
Stanford University
Stanford, California

ANALOG STUDIES OF THE LIMIT-CYCLE FUEL CONSUMPTION OF A SPINNING SYMMETRIC DRAG-FREE SATELLITE

by

Robert Farquhar

SUDAAR 276

May 1966

This work was performed in association with research sponsored by the National Aeronautics and Space Administration under Research Grant NsG 582

ANALOG STUDIES OF THE LIMIT-CYCLE FUEL CONSUMPTION OF A SPINNING SYMMETRIC DRAG-FREE SATELLITE

Introduction:

The lifetime of a drag-free satellite is directly related to the limit-cycle fuel-consumption rate of the control jets. By proper adjustment of control parameters, it is possible to maintain the fuel-consumption rate at an acceptable level. This report evaluates the results of an analog computer simulation for the case of a drag-free satellite which is spinning at a constant rate about its symmetry axis.

The limit-cycle fuel-consumption rate is employed as a performance criterion comparing an on-off control versus a pulse-width, pulse-frequency system. A lead-lag filter is used to derive rate information from the position measurements. Noise is added to these position measurements and its effect on the performance is also considered.

Analog Computer Simulation:

Derivation of the equations of motion and the control synthesis for the spinning drag-free satellite have been given by Lange.* Fig. 1 depicts the configuration for this case. The inertial coordinate system (x', y') is fixed with the x'-axis parallel to the direction of the drag force, and the body-fixed frame (x, y) rotates at a constant angular rate. The equations of motion in the body-fixed frame are

---

*"The Control and Use of Drag-Free Satellites" by B. Lange, Ph.D. Thesis, Dept. of Electrical Engineering, Stanford University, June 1964.

$$\left.\begin{aligned} \ddot{x} - \omega^2 x - 2\omega\dot{y} &= F_D \cos\omega t + F_{cx} \\ \ddot{y} - \omega^2 y + 2\omega\dot{x} &= -F_D \sin\omega t + F_{cy} \end{aligned}\right\} \tag{1}$$

where F_D is the magnitude of the drag acceleration (assumed constant for several limit-cycle periods), and F_{cx}, F_{cy} are the control accelerations along the x and y axes respectively. The substitutions

$$\xi = x + jy, \quad F_c = F_{cx} + j\,F_{cy}, \quad F_D = F_{Dx} + j\,F_{Dy} \tag{2}$$

transform Eq. (1) into the complex form

$$\ddot{\xi} + 2j\omega\dot{\xi} - \omega^2\xi = F_c + F_D \tag{3}$$

A second transformation

$$\eta \equiv \xi e^{j\omega t} \tag{4}$$

reduces Eq. (3) to

$$\ddot{\eta} = F_c e^{j\omega t} + F_D e^{j\omega t} \tag{5}$$

which is simply the equation of motion in the inertial frame. A standard linear feedback control is chosen as

$$F_c e^{j\omega t} = -K_v\dot{\eta} - K_p\eta = -K_v[\dot{\eta} + k\eta] \tag{6}$$

where $k \equiv K_p/K_v$

This control law is then transformed back into the rotating frame and becomes

$$F_c = -K_v[\dot{\xi} + (k + j\omega)\xi] \tag{7}$$

or in real form

$$\left.\begin{aligned} F_{cx} &= -K_v[\dot{x} - \omega y + kx] \\ F_{cy} &= -K_v[\dot{y} + \omega x + ky] \end{aligned}\right\} \tag{8}$$

Since this linear control makes the system stable for all positive values of the control gain, the linear gain element is replaced with a

relay control to operate the jet valves as suggested by Aizerman.* An alternate method is to approximate the linear control by a pulse-width, pulse-frequency system.

This system has been mechanized on the TR-48 analog computer where the problem is scaled to permit investigation of the limit-cycle behavior near the origin of the phase space. Details of the analog circuits are presented in the appendix. Block diagrams for the two control simulations are shown in Figs. 2-4.

Numerical values for the fixed parameters of this simulation were determined from practical considerations. The magnitude of the drag acceleration was taken to be $F_D = 7.17 \times 10^{-2}$ cm/sec^2, which corresponds to an altitude of 100 statute miles. This value probably will not be exceeded for most applications. The magnitude of the control acceleration was chosen as $F_c = 1$ cm/sec^2 which is about ten times the value for the drag acceleration. To eliminate the high-frequency noise spectrum, the cutoff frequency for the lag filter was set at 50 rad/sec. A nominal value of $k = 1$ sec^{-1} (k is not a fixed parameter), led to a value for the lag filter constant of $\alpha = 50$. Preliminary runs of the analog simulation were used to determine nominal values for the variable parameters. These values are listed in Table 1. The parameters were then varied, one at a time, about the nominal case and their effect on the fuel-consumption rate was recorded. Four different cases

---

*Absolute Stability of Control Systems by M. A. Aizerman and F. R. Gantmacher, Holden-Day, San Francisco, 1963.

were observed for every parameter variation. They were (See Fig. 2):

Case A: Rate gyro switch closed without noise inputs

Case B: Rate gyro switch open without noise inputs

Case C: Rate gyro switch closed with noise inputs

Case D: Rate gyro switch open with noise inputs.

To provide relative measure of performance, a normalized fuel-consumption rate is defined as

$$W \equiv \frac{\text{measured fuel-consumption rate}}{\text{theoretical minimum fuel-consumption rate}} \qquad (9)$$

where the theoretical minimum fuel-consumption rate is the value required to counteract the drag force. As there is generally a component of the thrust perpendicular to the direction of the drag when the satellite is rotating, the normalized fuel-consumption rate is always greater than unity.

Since the analog measurements showed some dispersion, it was necessary to run several trials for each data point to obtain an average value. The spread of the data varied approximately as $\triangle W \sim \pm 0.08(W-1)$. The primary reason for this proportionality was the method of estimating the fuel-consumption rate. The fuel-consumption rate was found by measuring the time for the control system to use up a specified amount of fuel. This meant that shorter averaging times were used at higher rates, causing a larger spread in the measurements. It should also be noted that additional variations were caused by the system's sensitivity to the pot settings.

Results for On-Off Control:

The normalized fuel-consumption rate as a function of the variable

parameters is presented in Figs. 5-8 (without noise inputs) and Figs. 9-13 (with noise inputs). It should be noted that high fuel-consumption rates usually correspond to large limit cycles. This is due to control pulses occurring on both sides of the deadzone as the limit-cycle size increases. Therefore, fuel is wasted since some control pulses actually augment the drag force. The frequency of these "bad firings" generally increases when noise is present. Large fuel-consumption rates for both high and low values of the feedback gain k are shown in Fig. 5 and Fig. 10. Since k is just the slope of the switching line, the limit-cycle size increases for large k. When k is small, the switching points are not precise and control pulses frequently occur at the wrong place. These effects are accentuated when noise is added. An interesting minimum exists near $\xi = 0.08$ cm in Fig. 6 and Fig. 11 when the rate gyro switch is open. This is primarily due to the increased importance of the gyro terms as x and y become large (see Eq. 8). The absence of the gyro terms degrades the accuracy of the rate information which increases fuel consumption. The minimum for the hysteresis δ shown in Fig. 12 may be due to improper switchings by the noise for small values of δ. In general it can be seen that although the fuel-consumption rate is usually higher with the rate gyro switch open, the difference is not too great for angular rates under 1 rad/sec, but increases rapidly for higher rates (see Fig. 8 and Fig. 13). It is also important to notice in Fig. 9 that the performance is very poor for noise levels higher than $\sigma = 2 \times 10^{-3}$ cm (deadzone to noise ratio $\cong$ 25).

Steady-state motion for the nominal case is represented by the phase planes of Fig. 14. A ten-second time interval was used for each photo. While occasional bad firings occur for case B, they are not nearly as severe as cases C and D.

Results for Pulse-Width, Pulse-Frequency Control (PWPF):

The normalized fuel-consumption rate graphs for this control are given in Figs. 15-19 (without noise inputs) and Figs. 20-25 (with noise inputs). Although the integrator gain τ is unimportant for cases A and B (see Fig. 15), it must be made large enough to be sure that the integrator does not track the noise as seen in Fig. 21. Scaling problems made it difficult to obtain data for higher angular rates in Fig. 19 and Fig. 25, but the phase plane behavior for these cases indicated results similar to Fig. 8 and Fig. 13. For the most part, the performance was slightly better with the rate gyro switch open. However, fuel consumption worsened rapidly without the rate cross-coupling as the vehicle was rotated faster than 1 rad/sec. Once again the graphs show that some improvement is derived by exceeding the nominal value of the trigger deadzone. It can also be seen that the PWPF system is about twenty times less sensitive to noise than the on-off control since the performance does not deteriorate until noise levels of about $\sigma = 4 \times 10^{-2}$ cm (trigger deadzone to noise ratio $\cong$ 1) are reached.

Phase planes for the nominal case are shown in Fig. 26. A thrust-direction history for the nominal case is given in Table 2 where it can be seen that the larger thrust component usually opposes the drag force.

Conclusions:

This simulation has shown that the pulse-width, pulse-frequency control system has superior noise-rejection characteristics in comparison to strictly on-off control. In addition, the PWPF system is more economical even without noise inputs.

Since only small differences were noted when the rate gyro switch was open, this portion of the control could be removed to simplify the system. However, this change is only warranted when the angular rates are sufficiently small.

The simulation has also shown that both control systems automatically commutate the jets fixed on the rotating vehicle so that they fire to oppose the drag force, except that there is a small control component perpendicular to the drag direction which stabilizes the cross-axis motion. Furthermore, the control systems do not require measurements of the magnitude or direction of the drag force.

TABLE 1. Nominal Values for Variable Parameters

1.	Feedback gain:	$k = 1 \text{ sec}^{-1}$
2.	Deadzone:	$\xi = 0.05$ cm
3.	Hysteresis:	$\delta = 0.038$ cm
4.	Angular rate:	$\omega = 1$ rad/sec
5.	Integrator gain:	$\tau = 0.75$ sec
6.	Noise Level:	
	(on-off)	$\sigma_o = 1.418 \times 10^{-3}$ cm
	(PWPF)	$\sigma_o = 2.270 \times 10^{-2}$ cm

TABLE 2. Thrust direction history for PWPF control
(Duration: 6 cycles or 37.7 sec.)

Angle between thrust and drag (thrust component opposing drag)	Case			
	(Without Noise)		(With Noise)	
	A With Gyro	B Without Gyro	C With Gyro	D Without Gyro
± 45°	35	33	38	36
± 45° → ± 60°	7	9	9	10
± 60° → ± 90°	6	2	12	15
Bad firings (no thrust component opposing drag)	2	2	8	10
Total firings	50	46	67	71

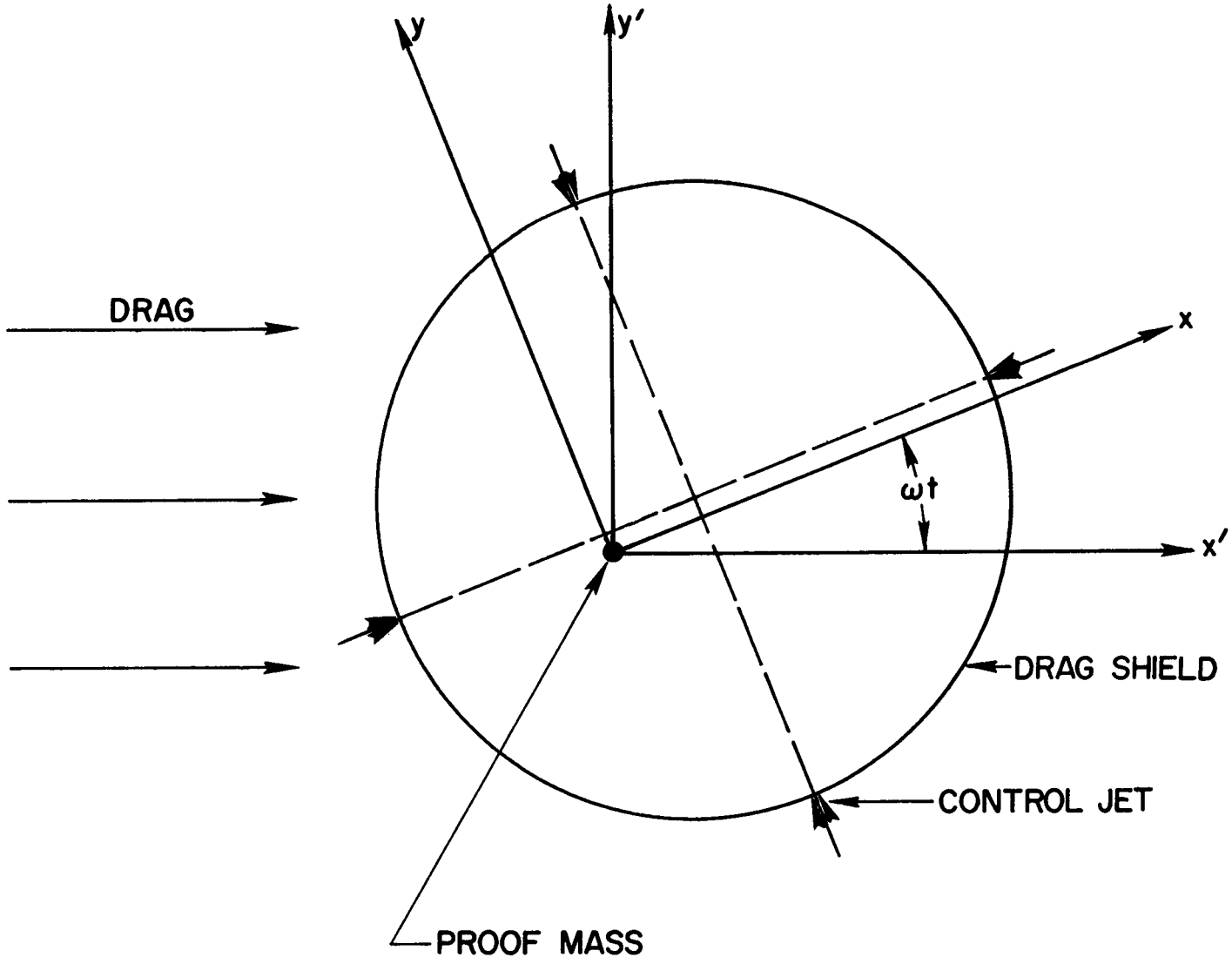

Fig. 1. Spinning Drag-Free Satellite

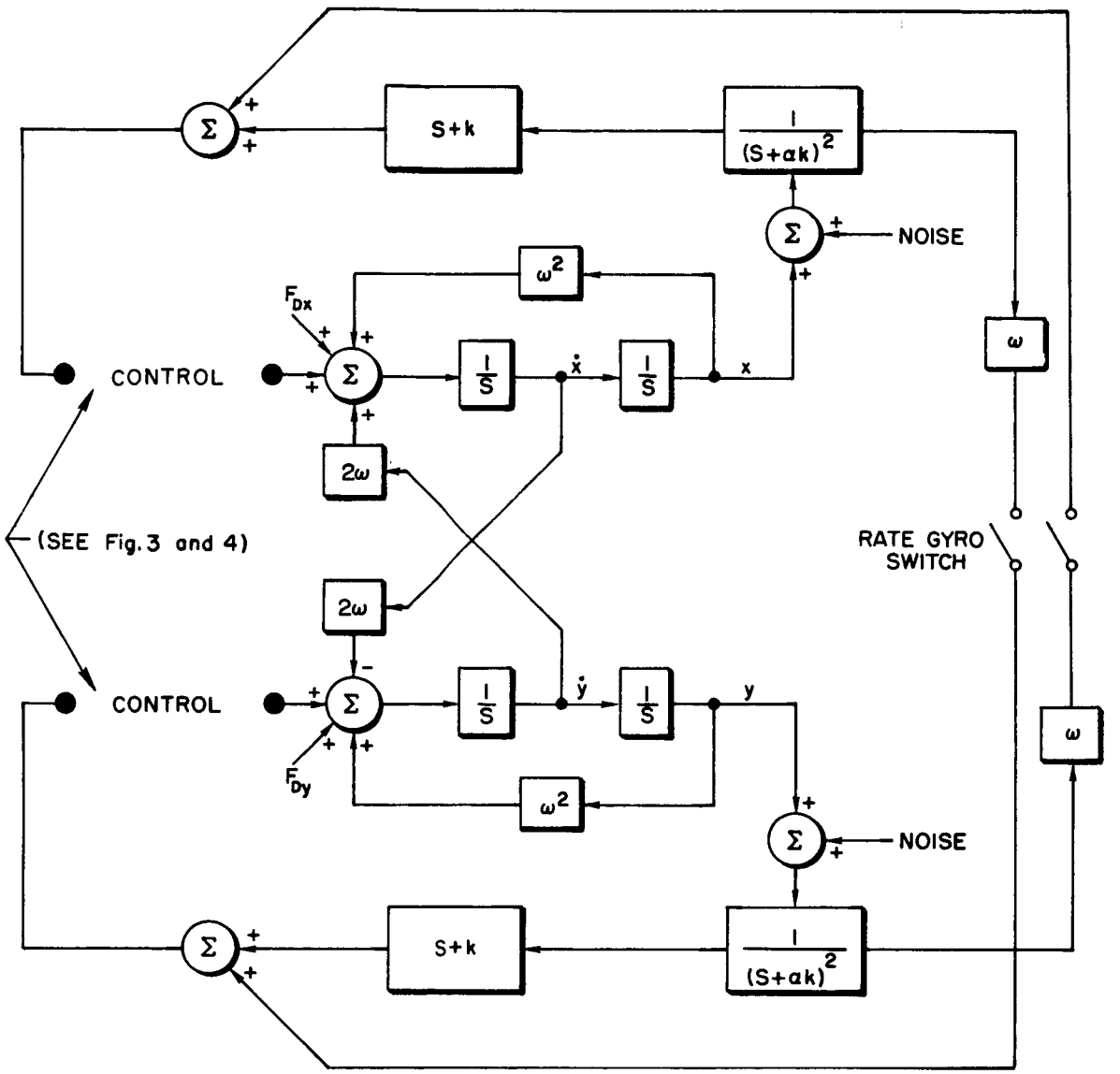

Fig. 2. Block Diagram of Control Simulation

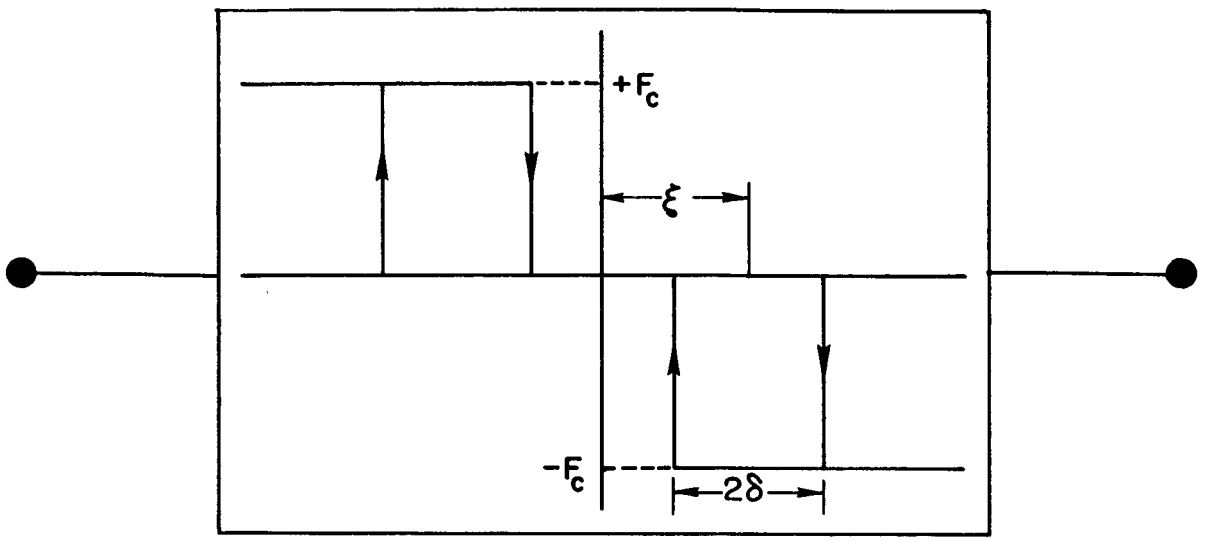

Fig. 3. On-Off Control

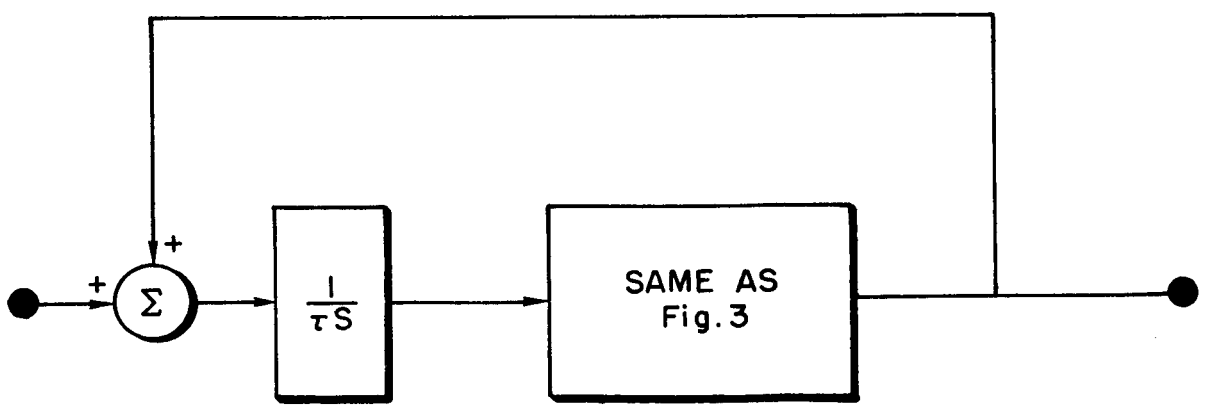

Fig. 4. Pulse-Width, Pulse-Frequency Control

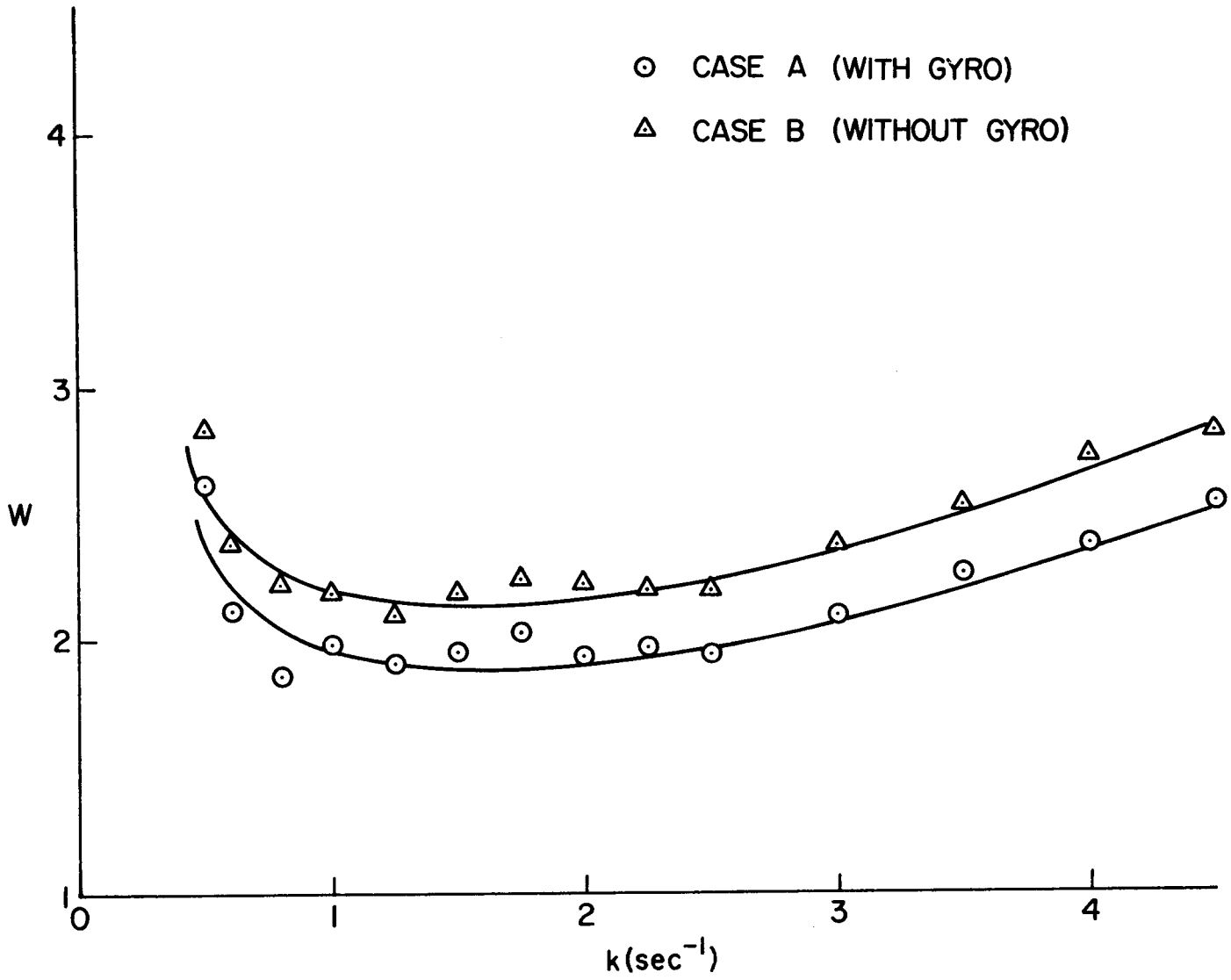

Fig. 5. Normalized Fuel-Consumption Rate Vs Feedback Gain (On-Off Control Without Noise)

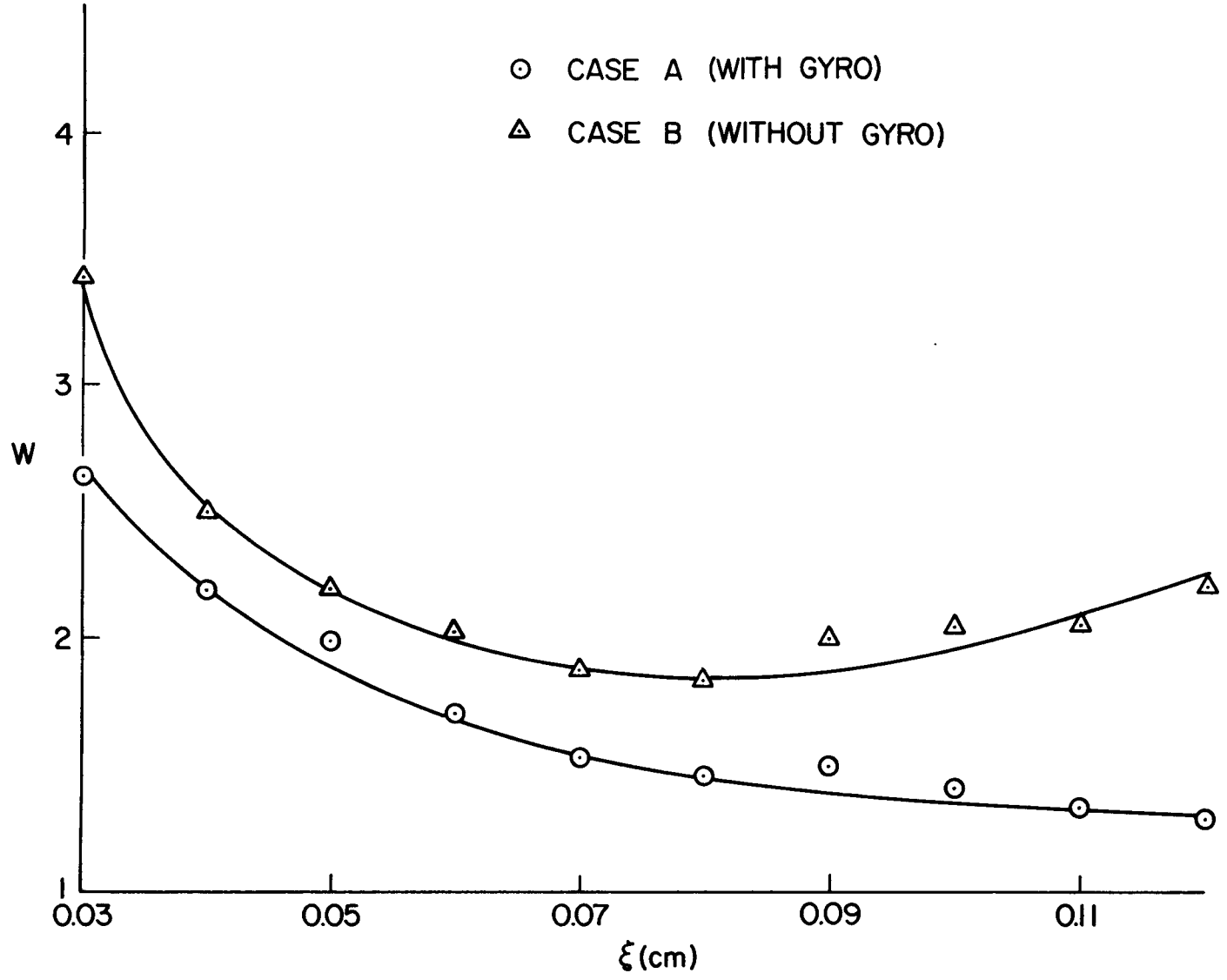

Fig. 6. Normalized Fuel-Consumption Rate Vs Deadzone (On-Off Control Without Noise)

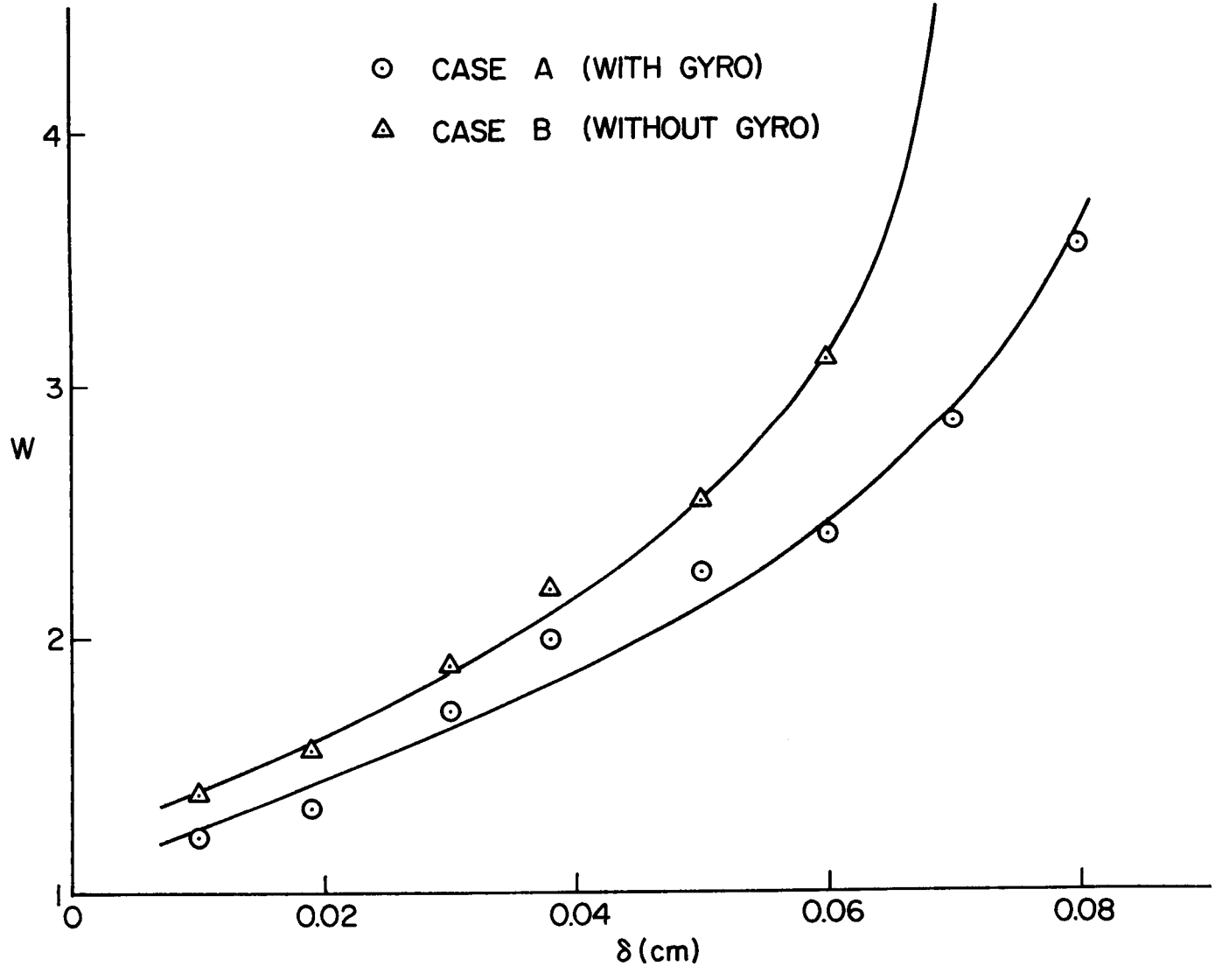

Fig. 7. Normalized Fuel-Consumption Rate Vs Hysteresis (On-Off Control Without Noise)

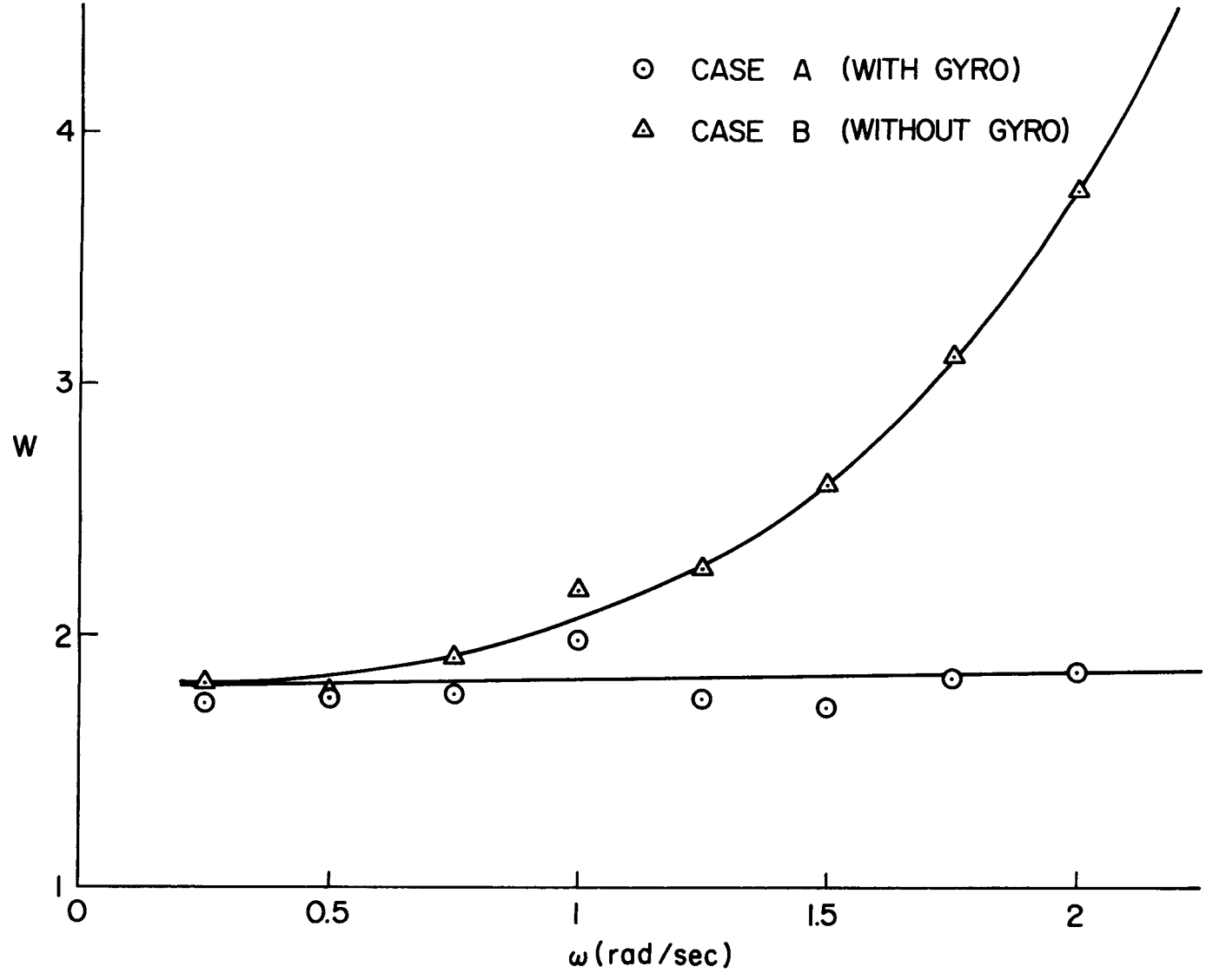

Fig. 8. Normalized Fuel-Consumption Rate Vs Angular Rate (On-Off Control Without Noise)

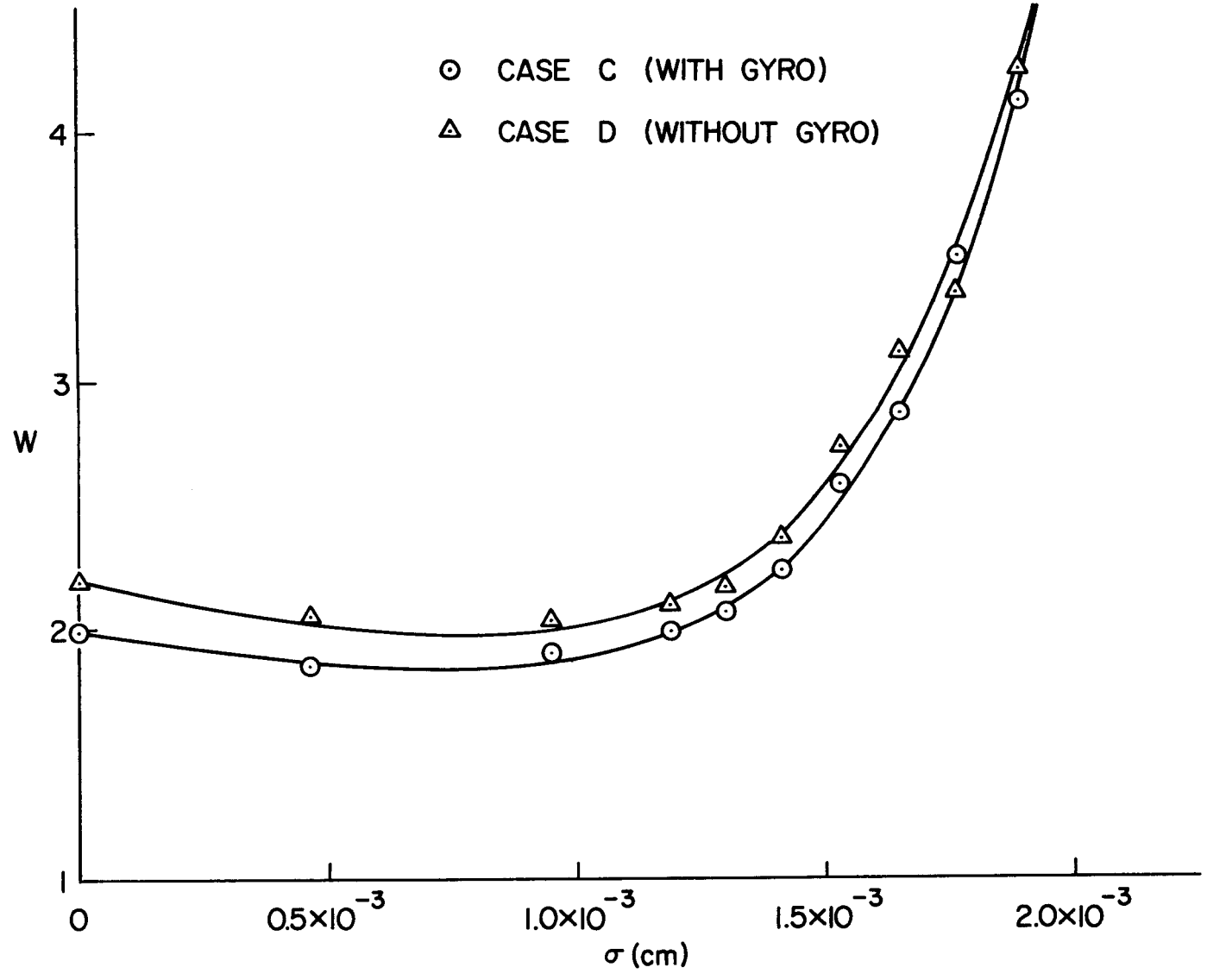

Fig. 9. Normalized Fuel-Consumption Rate Vs Noise Level (On-Off Control With Noise)

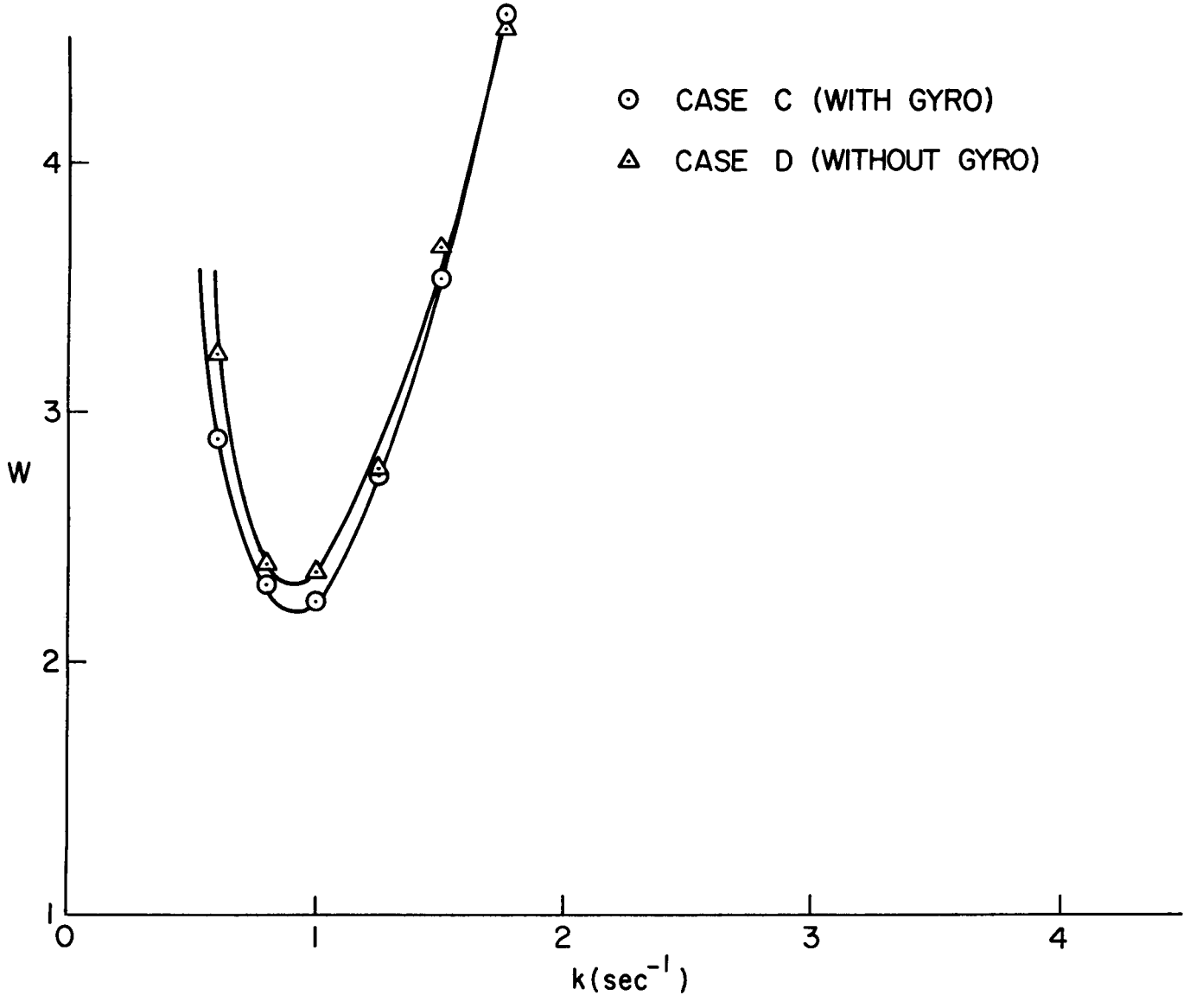

Fig. 10. Normalized Fuel-Consumption Rate Vs Feedback Gain (On-Off Control With Noise)

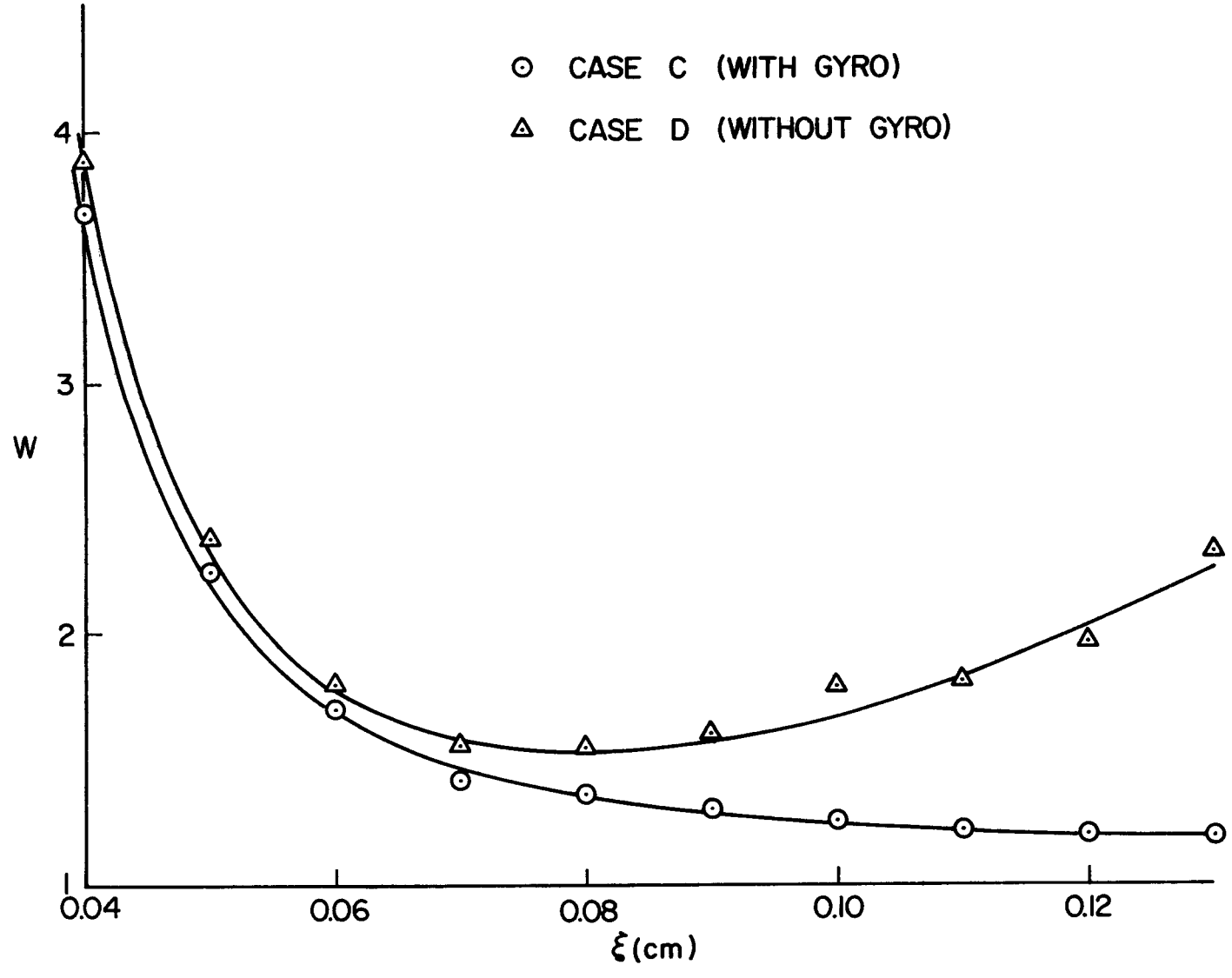

Fig. 11. Normalized Fuel-Consumption Rate Vs Deadzone (On-Off Control With Noise)

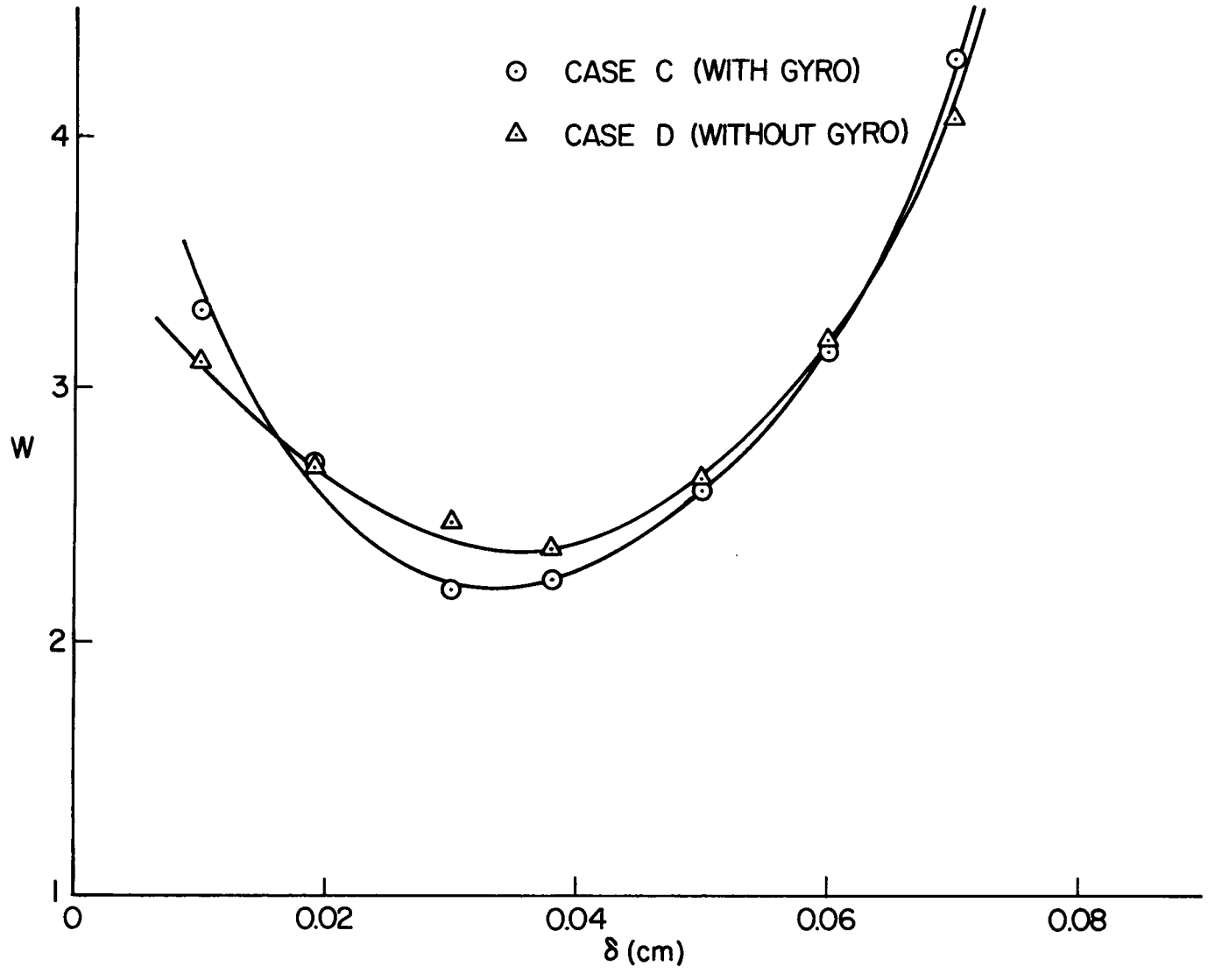

Fig. 12. Normalized Fuel-Consumption Rate Vs Hysteresis (On-Off Control With Noise)

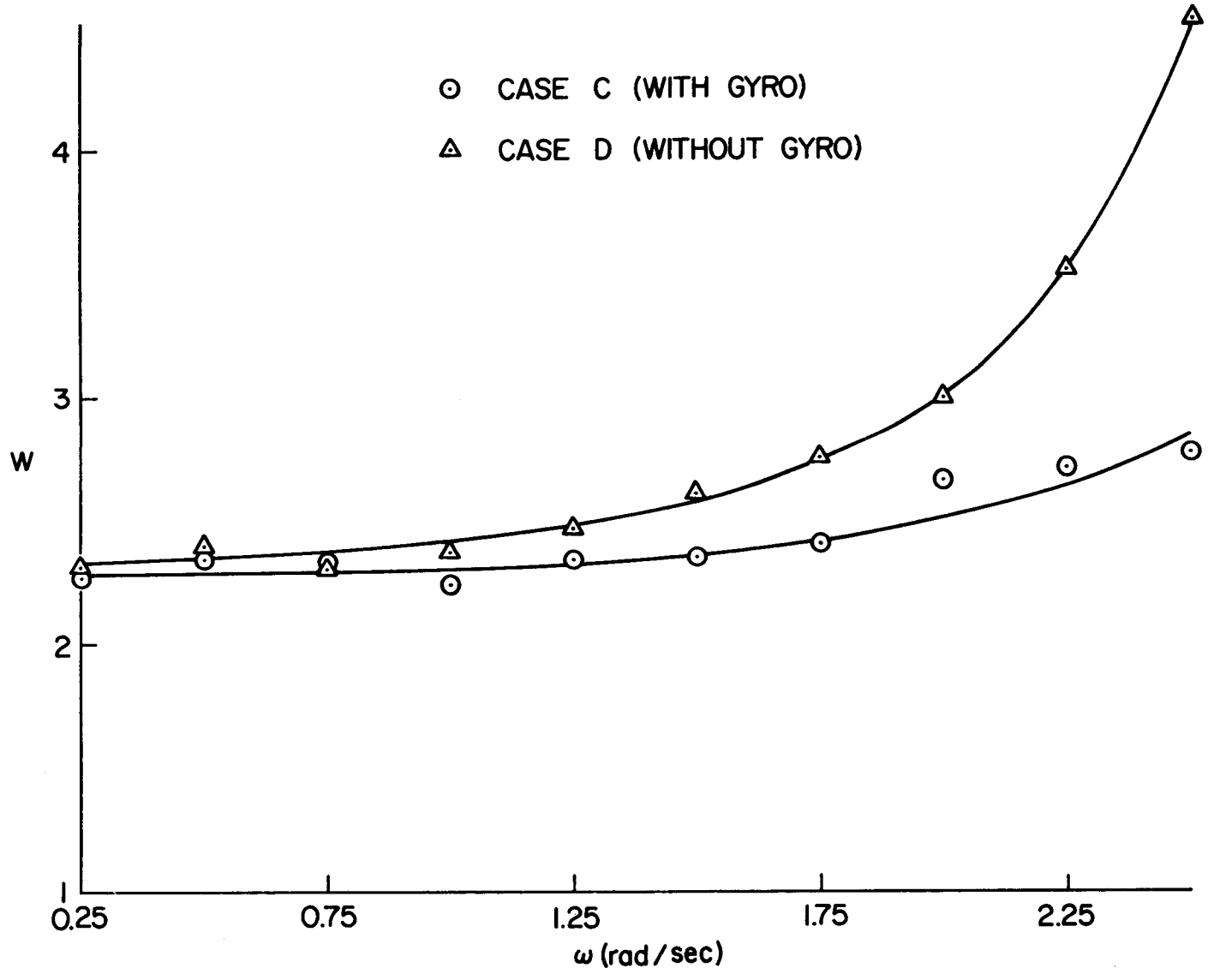

Fig. 13. Normalized Fuel-Consumption Rate Vs Angular Rate (On-Off Control With Noise)

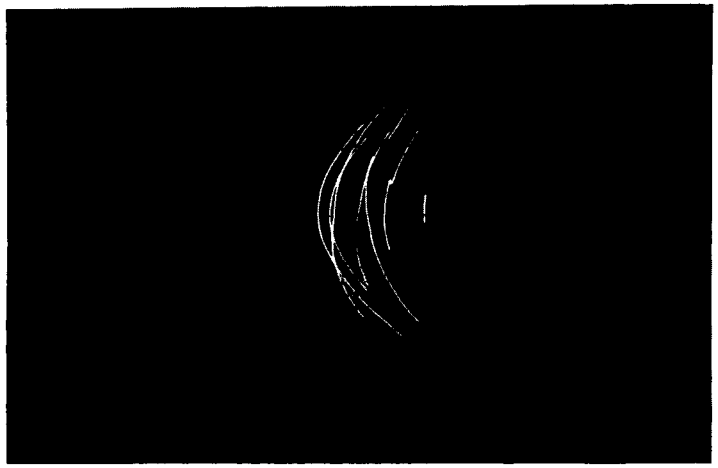

Case A
(Gyro, Without Noise)

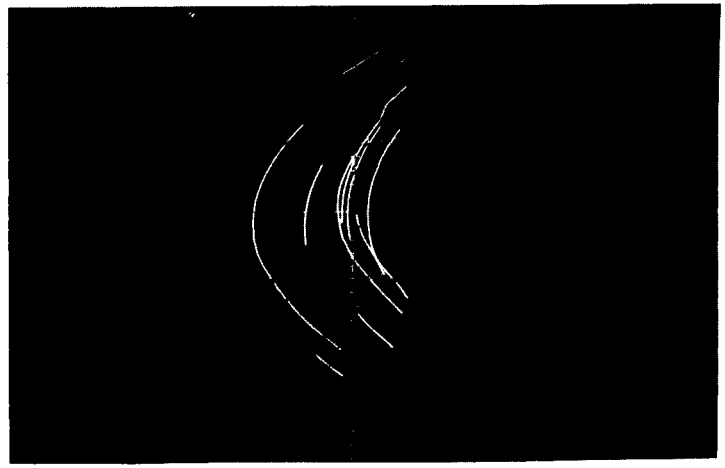

Case B
(No Gyro, Without Noise)

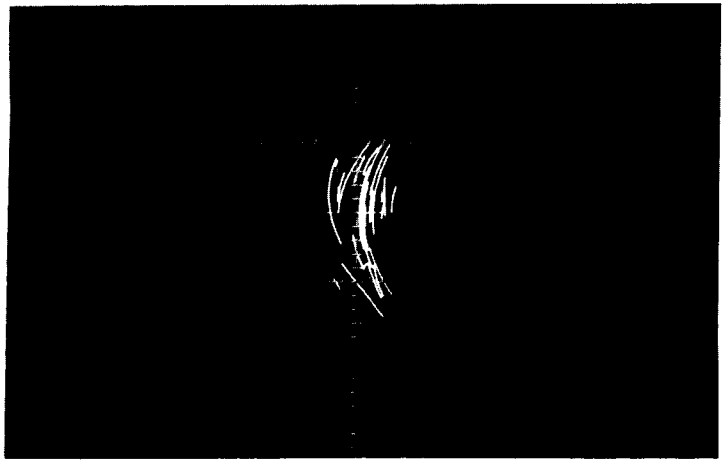

Case C
(Gyro, With Noise)

Case D
(No Gyro, With Noise)

Fig. 14. Phase Planes of $\dot{x}'$ Vs x' For On-Off Control (Grid Size: 0.04 cm)

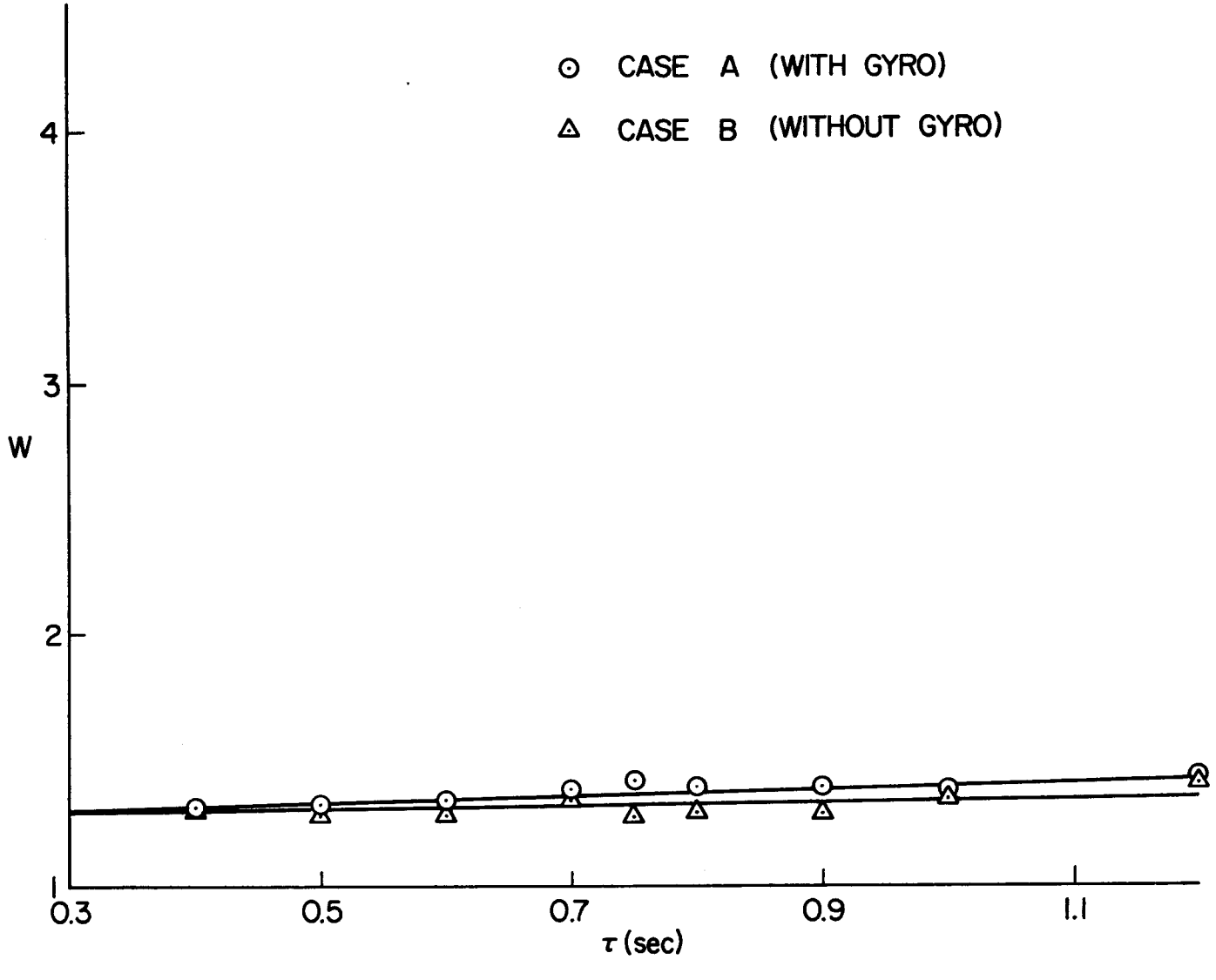

Fig. 15. Normalized Fuel-Consumption Rate Vs Integrator Gain (PWPF Control Without Noise)

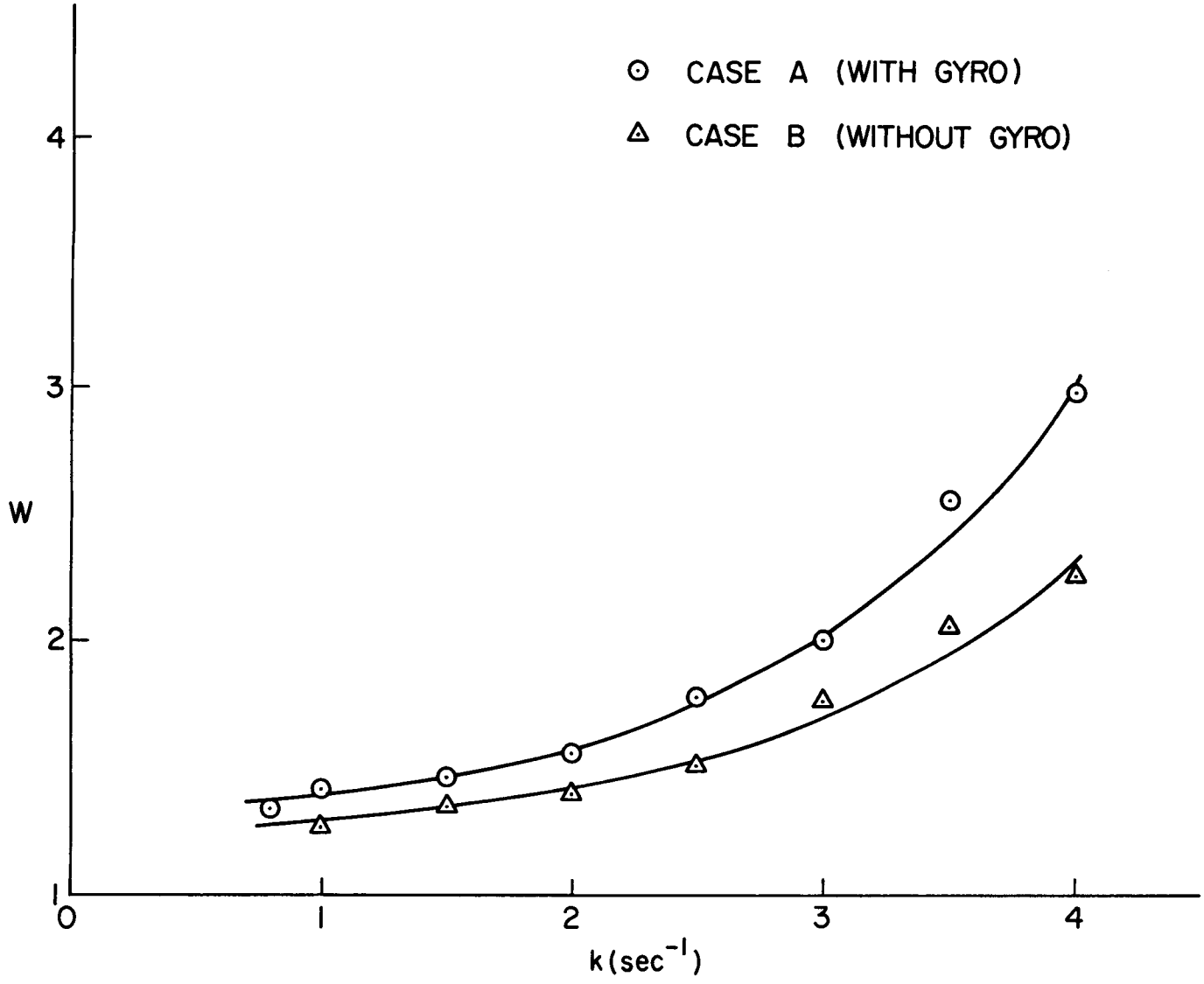

Fig. 16. Normalized Fuel-Consumption Rate Vs Feedback Gain (PWPF Control Without Noise)

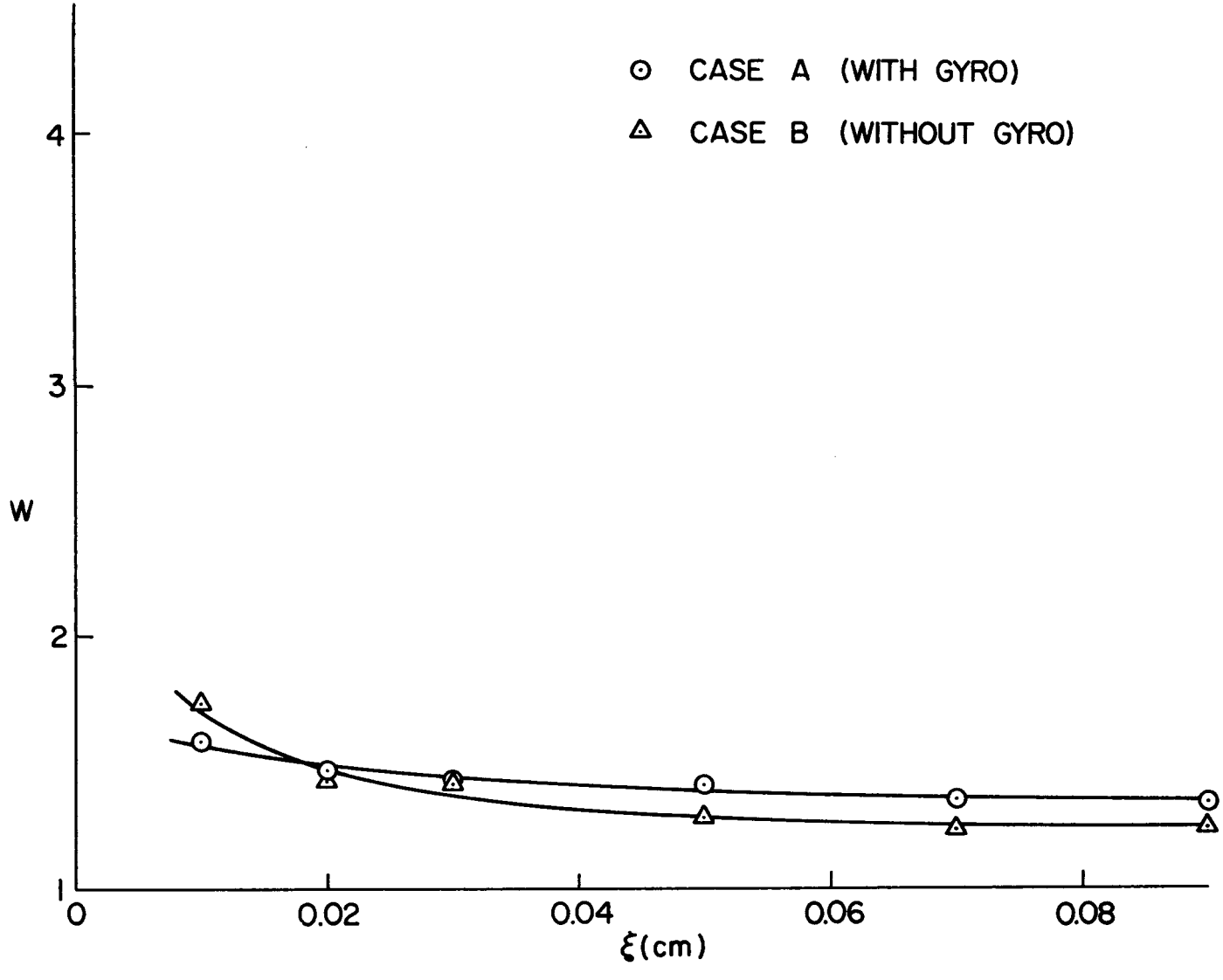

Fig. 17. Normalized Fuel-Consumption Rate Vs Trigger Deadzone (PWPF Control Without Noise)

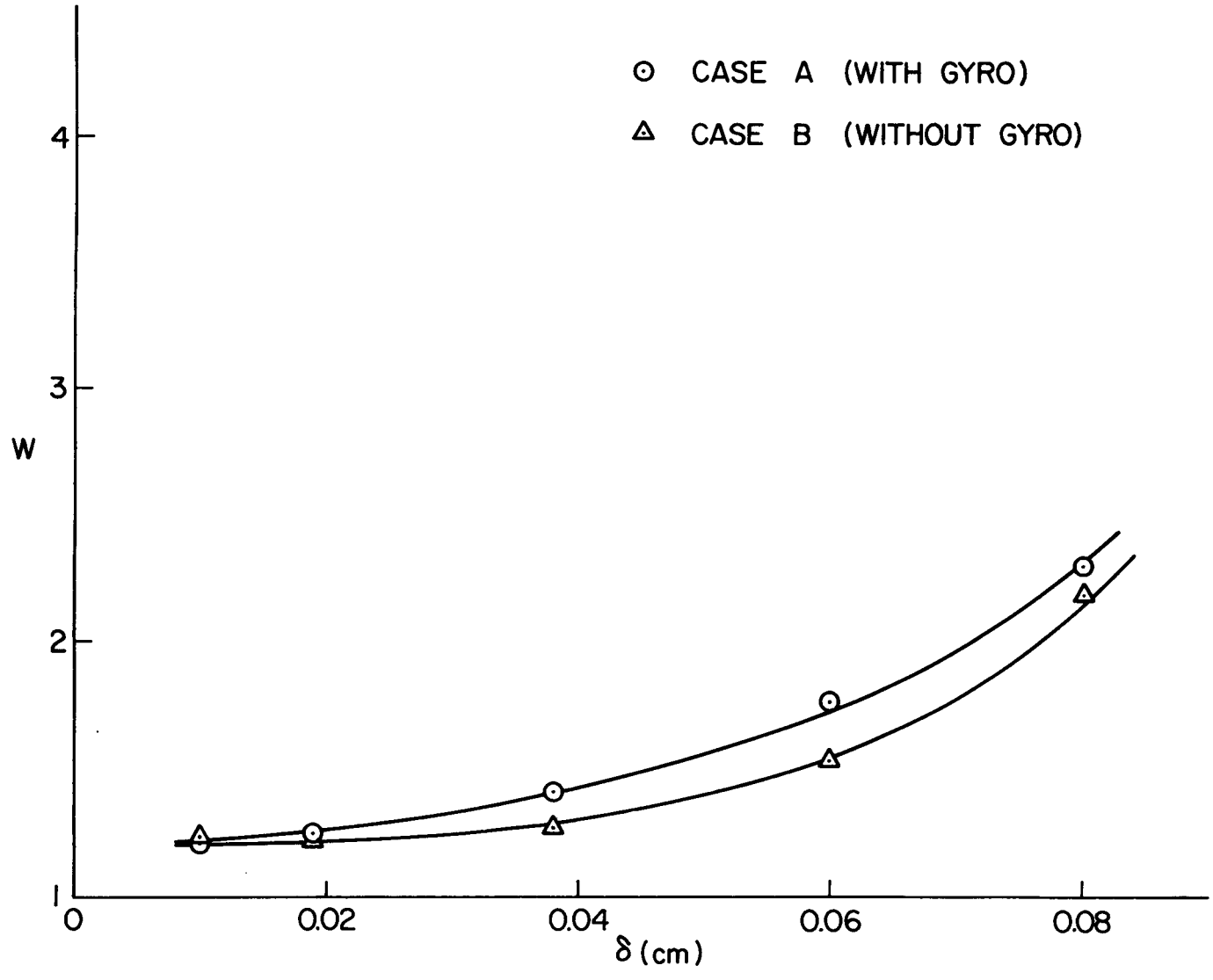

Fig. 18. Normalized Fuel-Consumption Rate Vs Hysteresis (PWPF Control Without Noise)

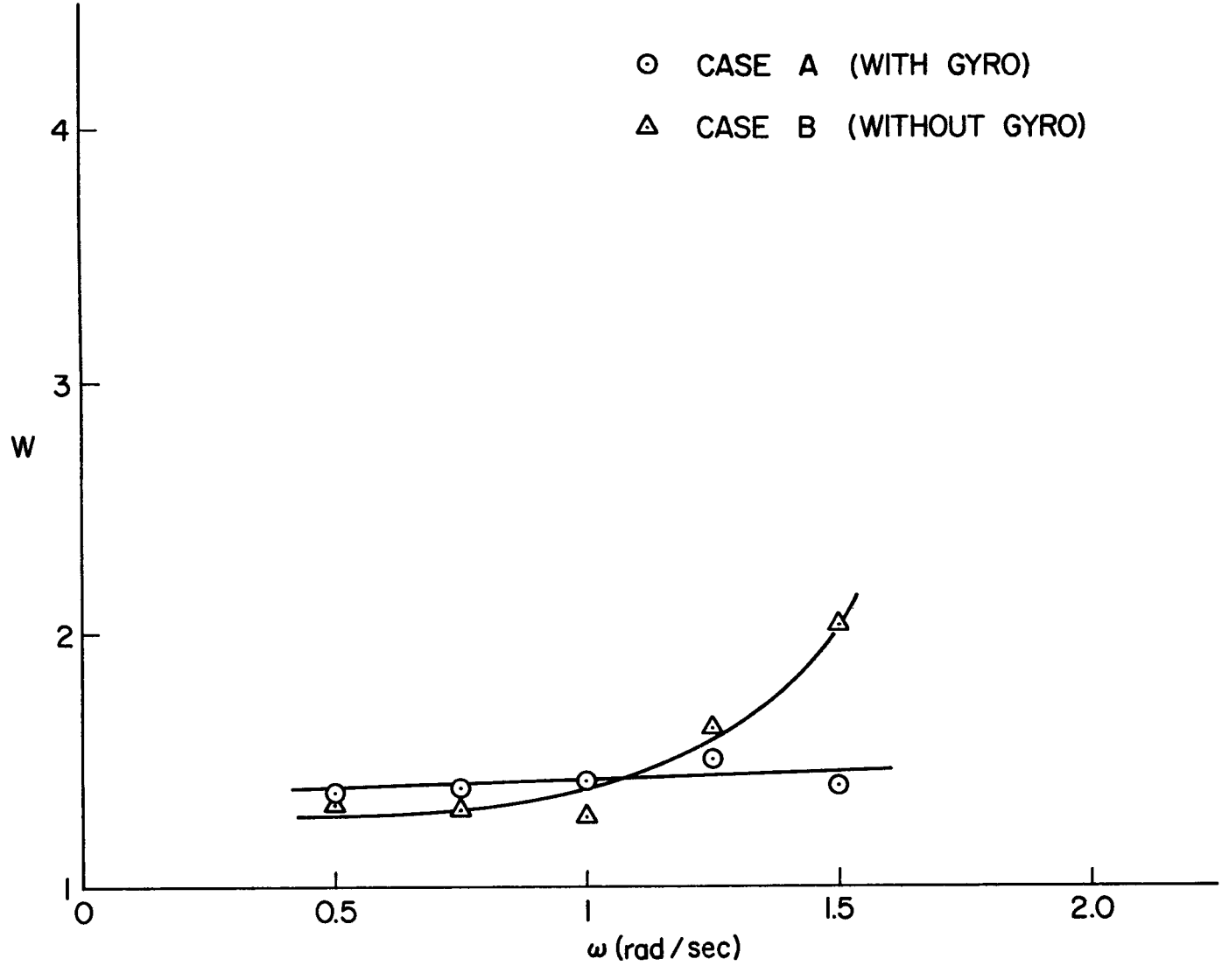

Fig. 19. Normalized Fuel-Consumption Rate Vs Angular Rate (PWPF Control Without Noise)

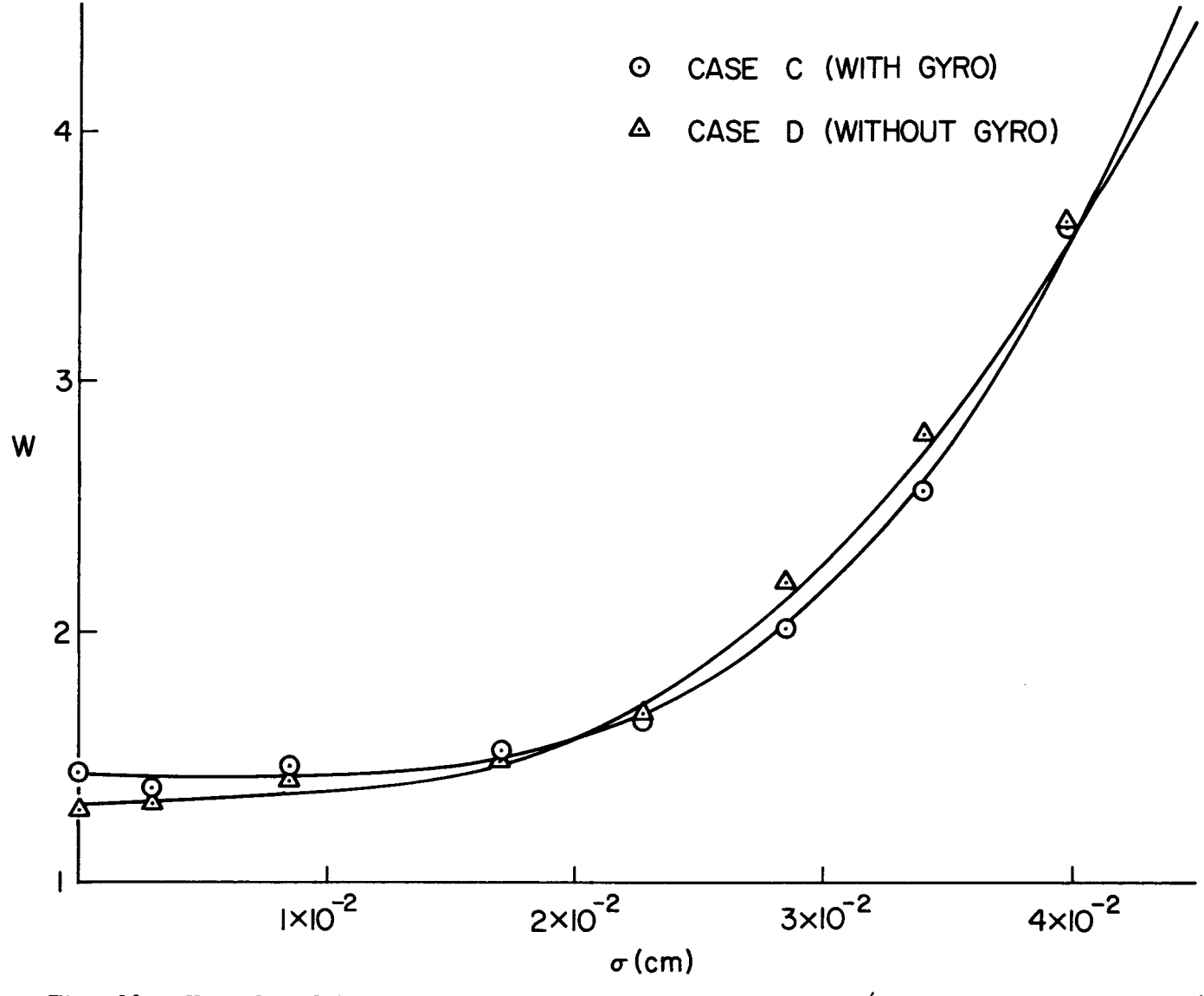

Fig. 20. Normalized Fuel-Consumption Rate Vs Noise Level (PWPF Control With Noise)

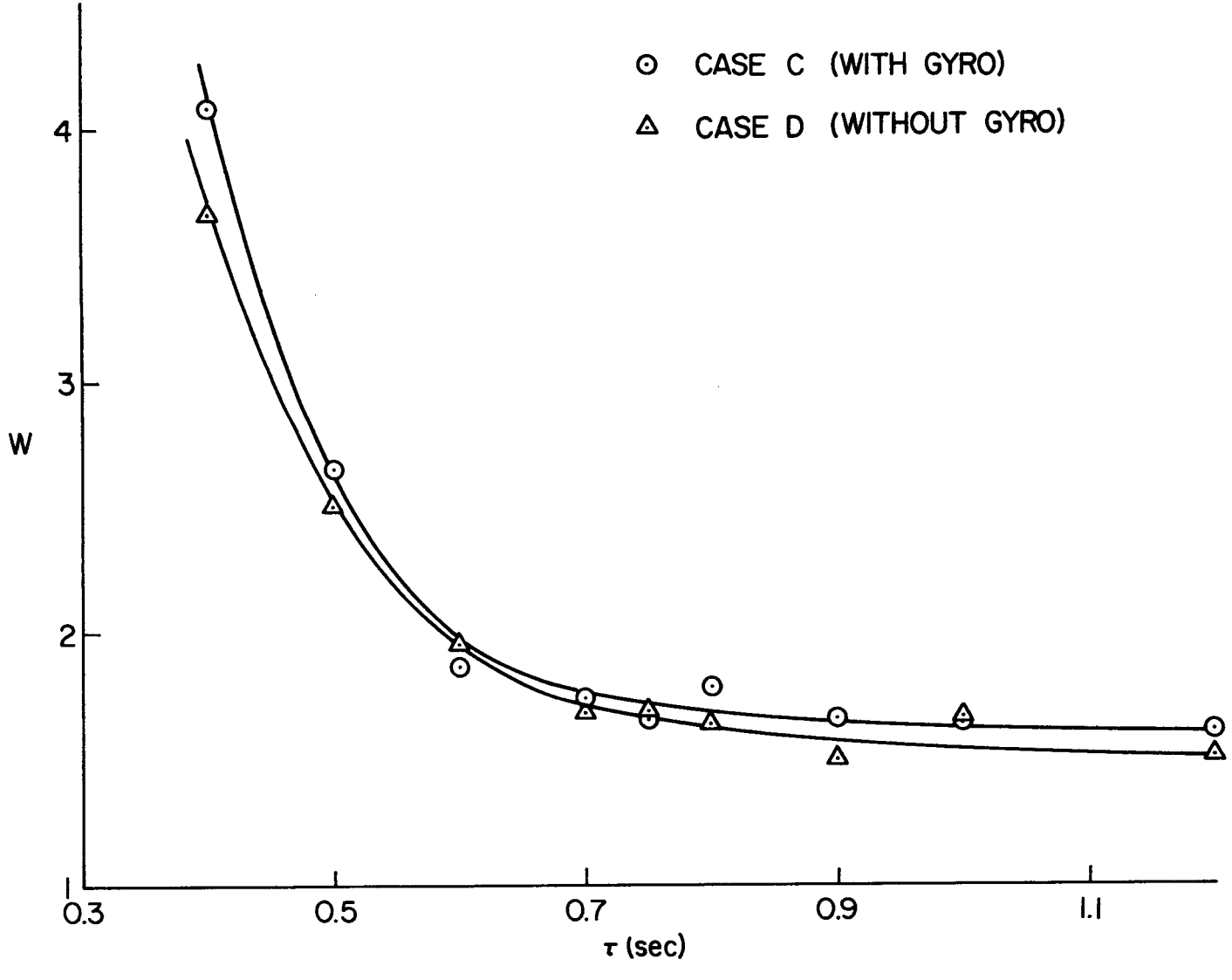

Fig. 21. Normalized Fuel-Consumption Rate Vs. Integrator Gain (PWPF Control With Noise)

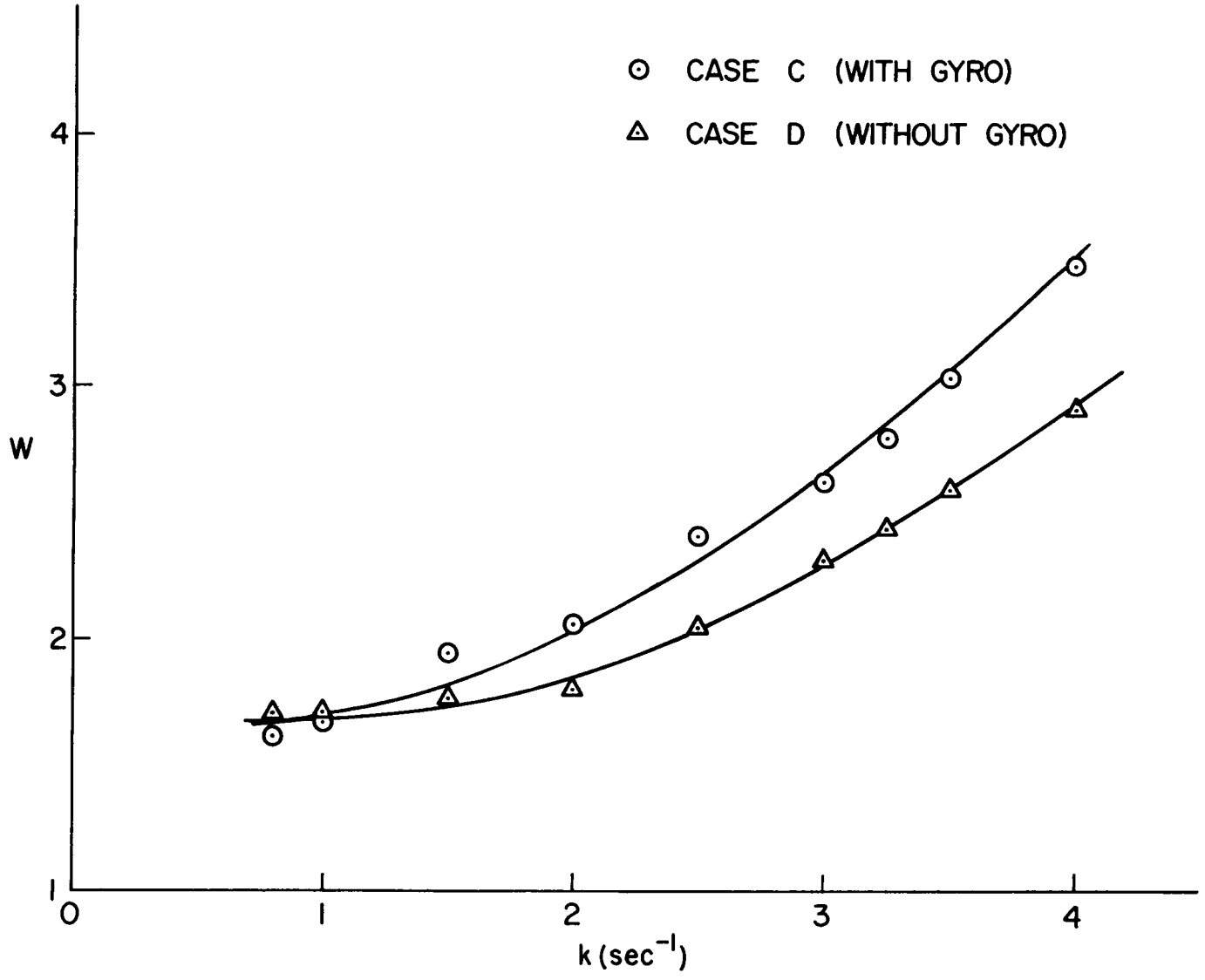

Fig. 22. Normalized Fuel-Consumption Rate Vs Feedback Gain (PWPF Control With Noise)

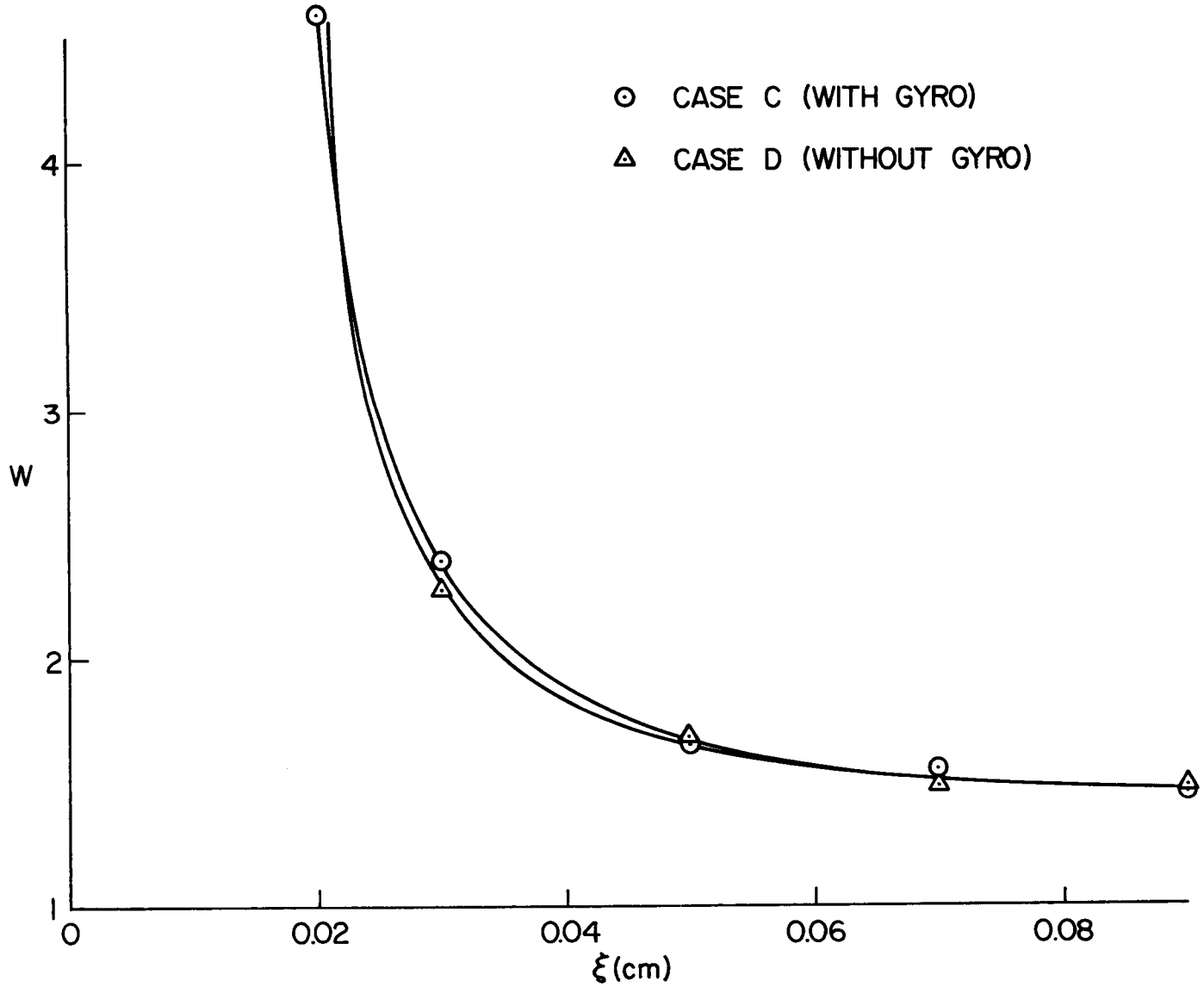

Fig. 23. Normalized Fuel-Consumption Rate Vs Trigger Deadzone (PWPF Control With Noise)

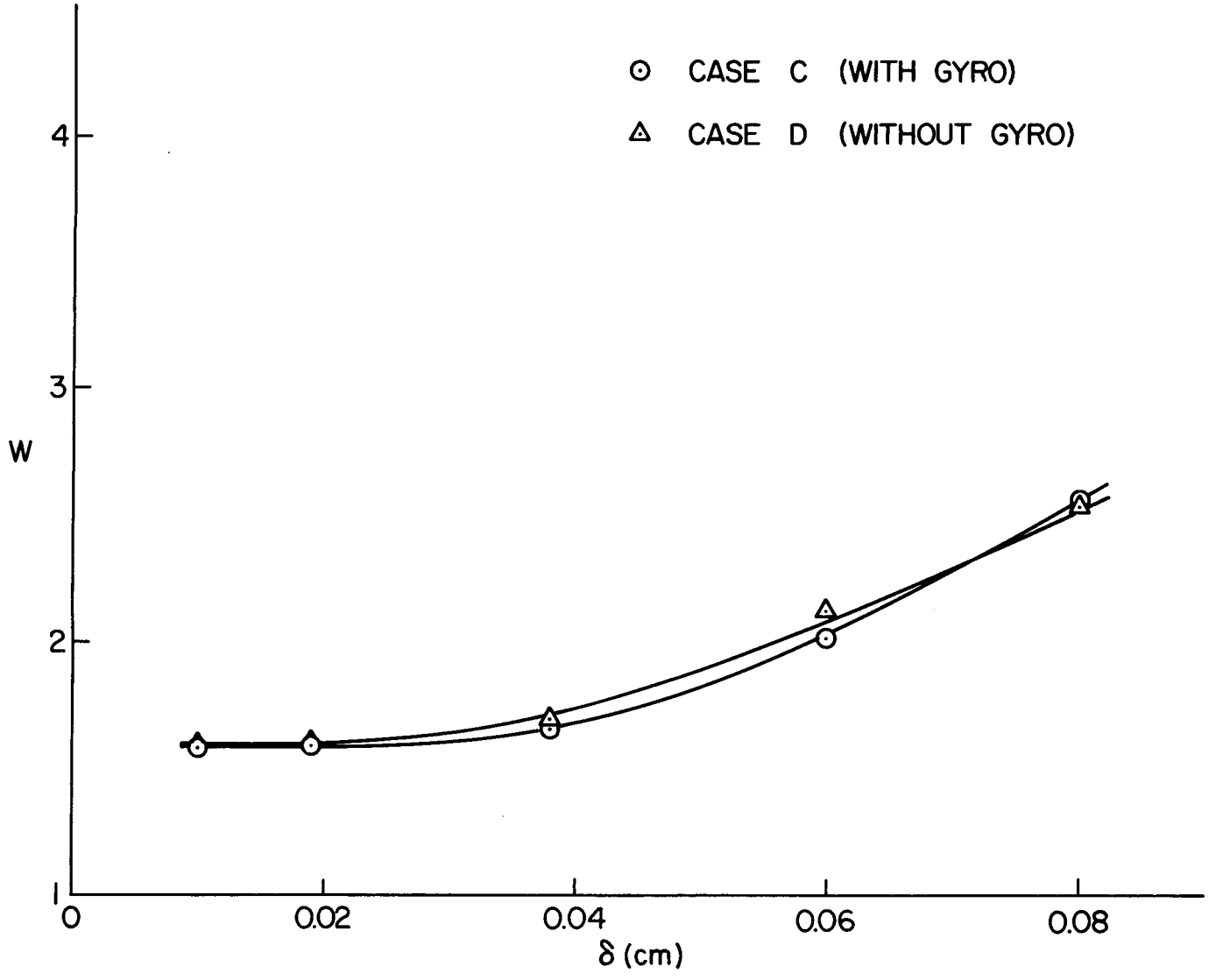

Fig. 24. Normalized Fuel-Consumption Rate Vs Hysteresis (PWPF Control With Noise)

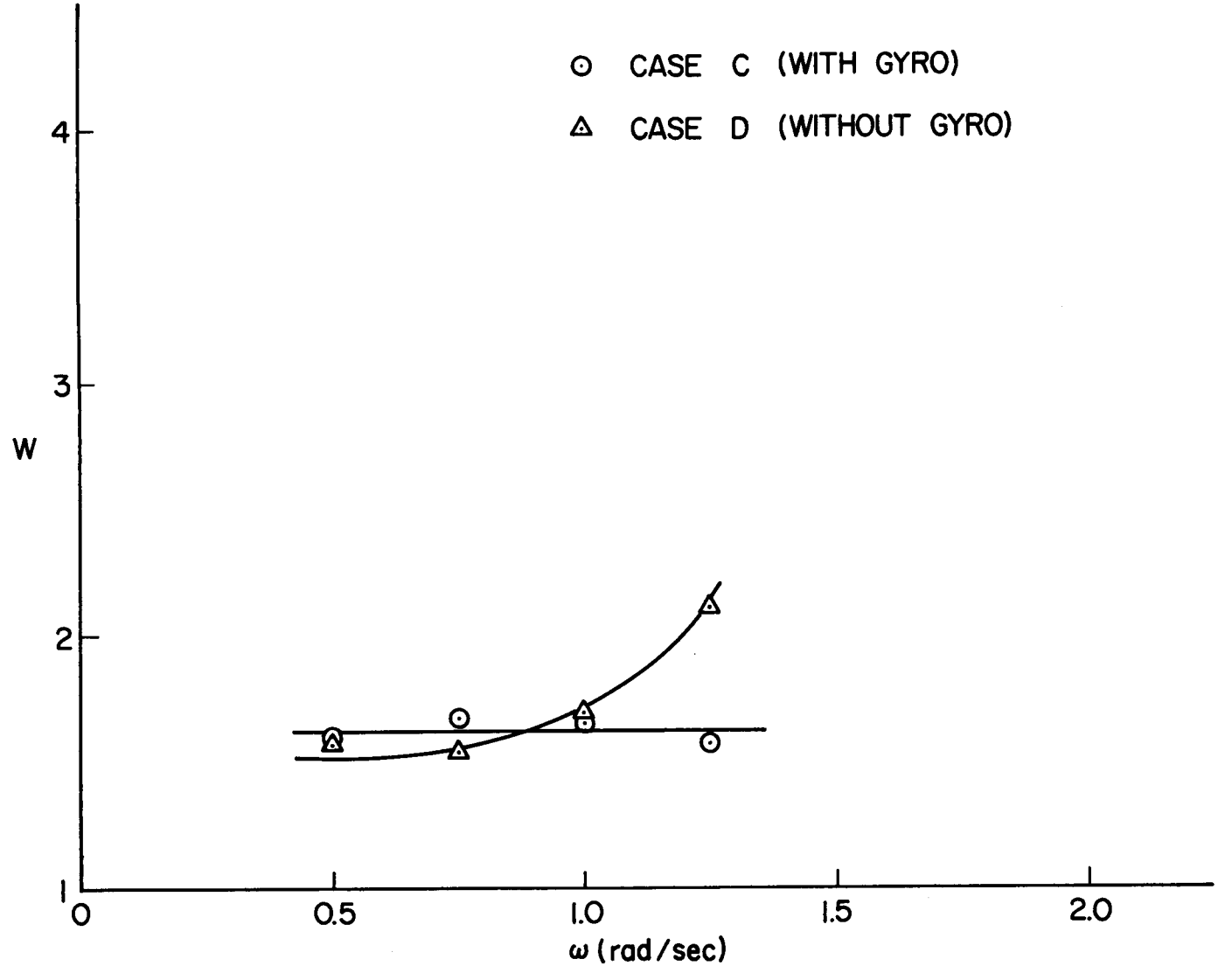

Fig. 25. Normalized Fuel-Consumption Rate Vs Angular Rate (PWPF Control With Noise)

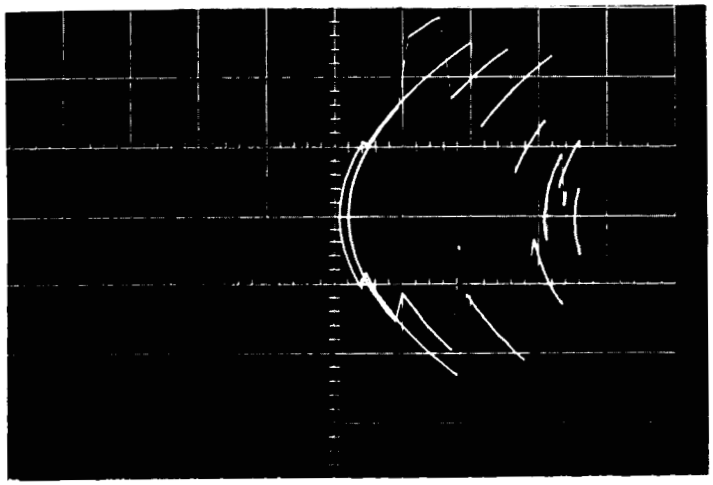

Case A
(Gyro, Without Noise)

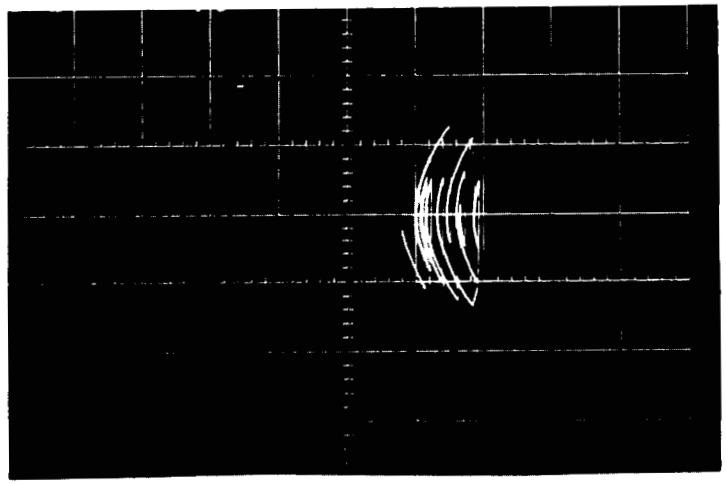

Case B
(No Gyro, Without Noise)

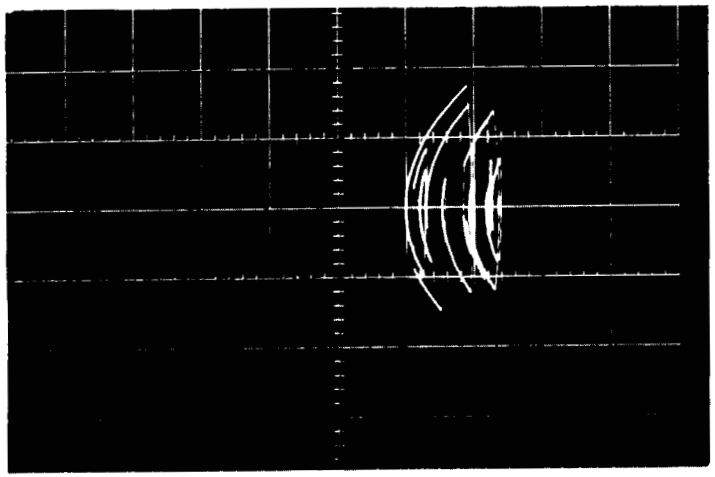

Case C
(Gyro, With Noise)

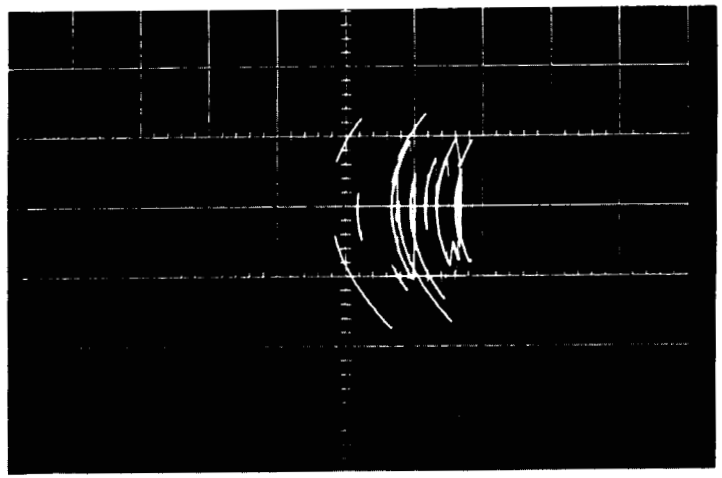

Case D
(No Gyro, Without Noise)

Fig. 26. Phase Planes of $\dot{x}'$ Vs x' for PWPF Control (Grid Size: 0.04 cm)

APPENDIX ANALOG CIRCUITS

The two TR-48 computers used in this simulation are shown in Fig. A-1. The analog circuits are given in Figs. A-2 to A-7. Since the control simulation is identical for each channel of the dual axis system shown in Fig. A-3, the two channels are shown simultaneously in Figs. A-4 to A-6. Although it is not shown in the figures, noise should also be added to the rate gyro inputs. Satisfactory operation in the limit cycle mode was obtained by using an amplitude scale factor of 0.02 cm per volt. The integrators were run at ten times their normal rate with a time scale factor of $\beta = 10$. This prevented amplifier overload and made it possible to run the problem in real time. Due to inherent time-delay in the computer, it was also necessary to set initial conditions on the integrator of the filter in Fig. A-4 to prevent initial overload.

The noise generator used for this study was manufactured by Electronic Associates Incorporated (designated Model 201A). The spectral density was determined by passing the noise through a narrow band-pass filter and then measuring the variance of the filter output. As the order of the lag filter was increased, the contribution of the non-uniform portion of the generator spectrum diminished. The value of the uniform spectral density converged to $N_o \cong 1.89 \times 10^{-3}$ $(\text{volts})^2/(\text{rad/sec})$ for a third-order lag filter with a cutoff frequency of 100 rad/sec. The operating manual for the noise generator claims that there is a 95% certainty that the measured value of spectral density is

within 2.5% of the true value.

The pot settings for the discontinuous control(Fig. A-6) did not behave linearly and it was necessary to find them by experimentation. Pots one and two fixed the operating level at ten volts since the network did not perform properly at low voltage levels. Pots three and four set the deadzone size while pot five determined the amount of hysteresis. A relay was used to cut off small currents which leaked through the high gain amplifier. The relay also determines the sign and magnitude of the control signal.

The fuel-consumption rate was found by simply integrating the control impulse until the integrator reached a specified value. The time taken to attain this value was measured by another integrator which acted as a clock.

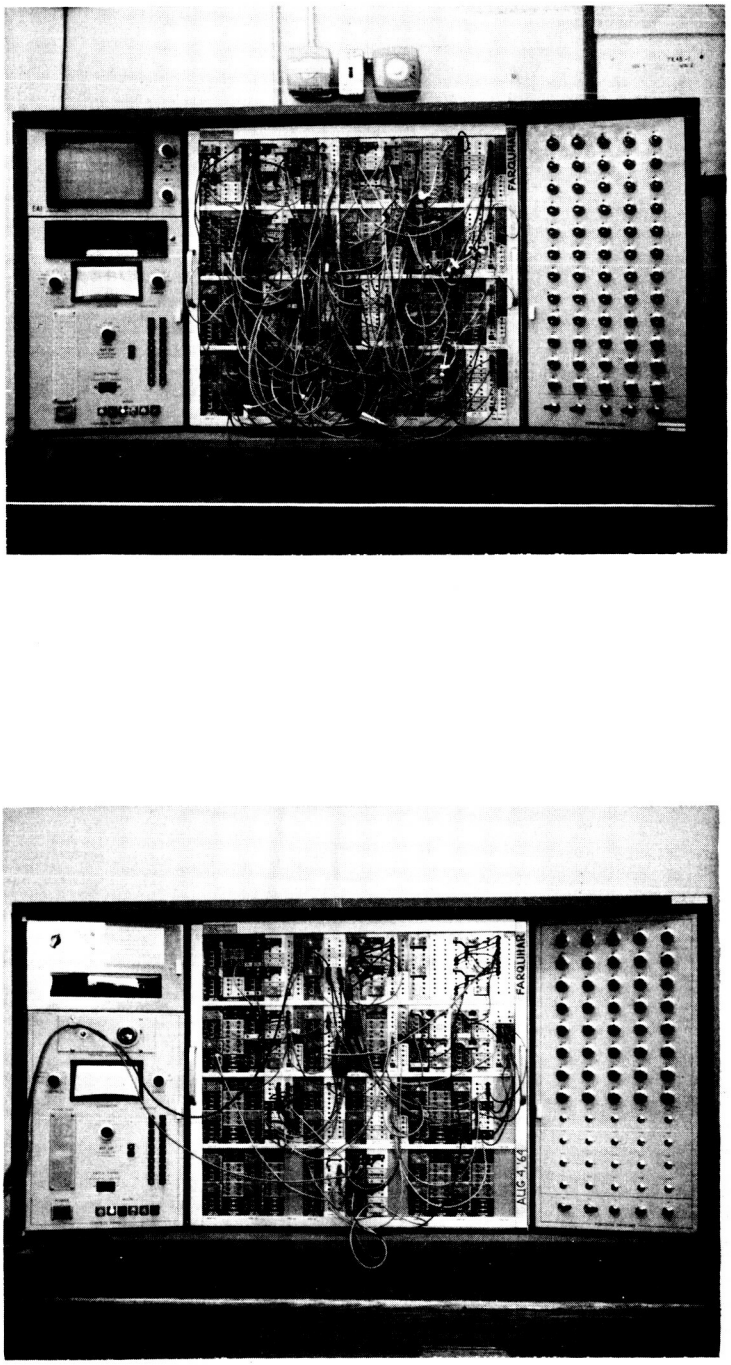

Fig. A-1. TR-48 Analog Computers

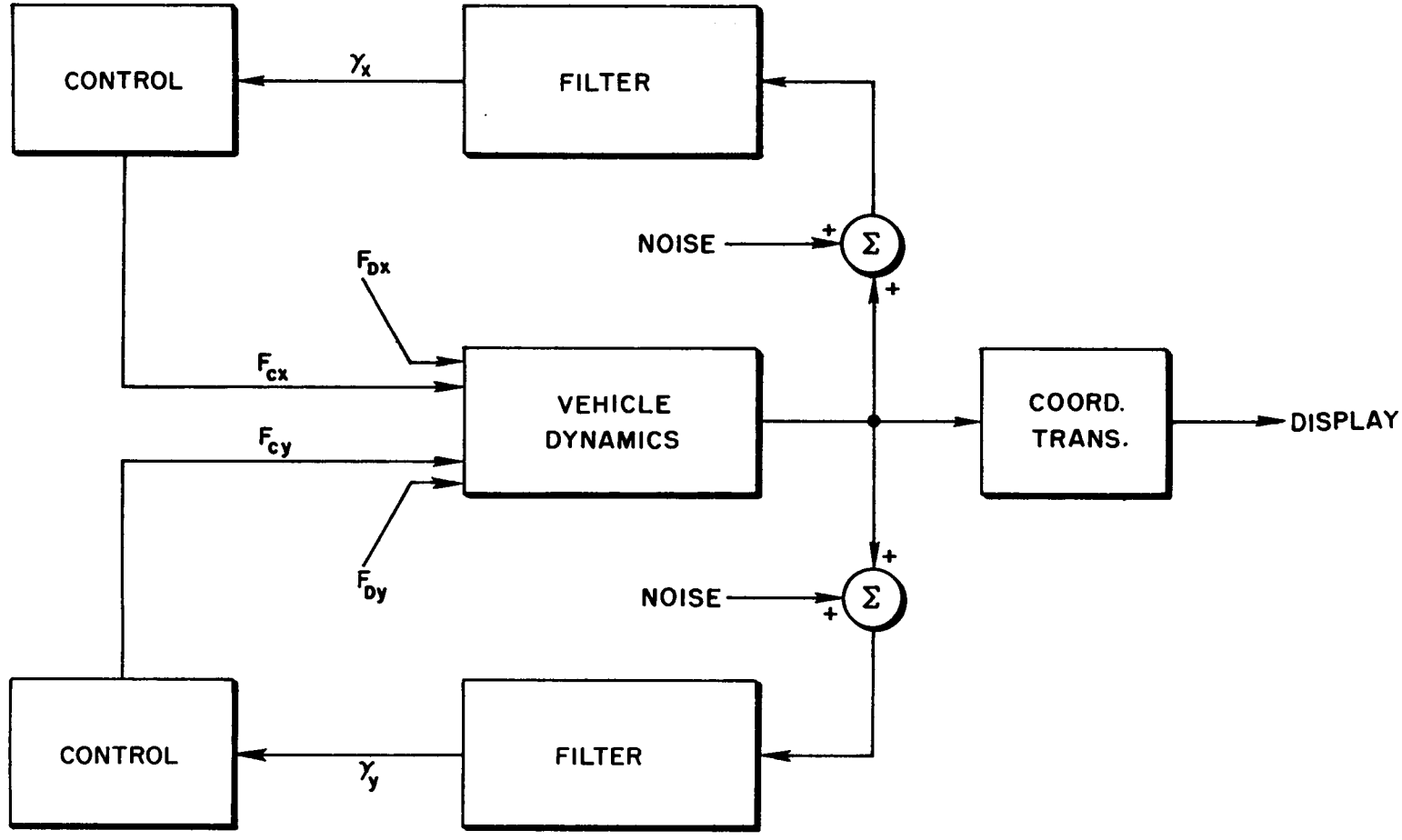

Fig. A-2. Analog Simulation

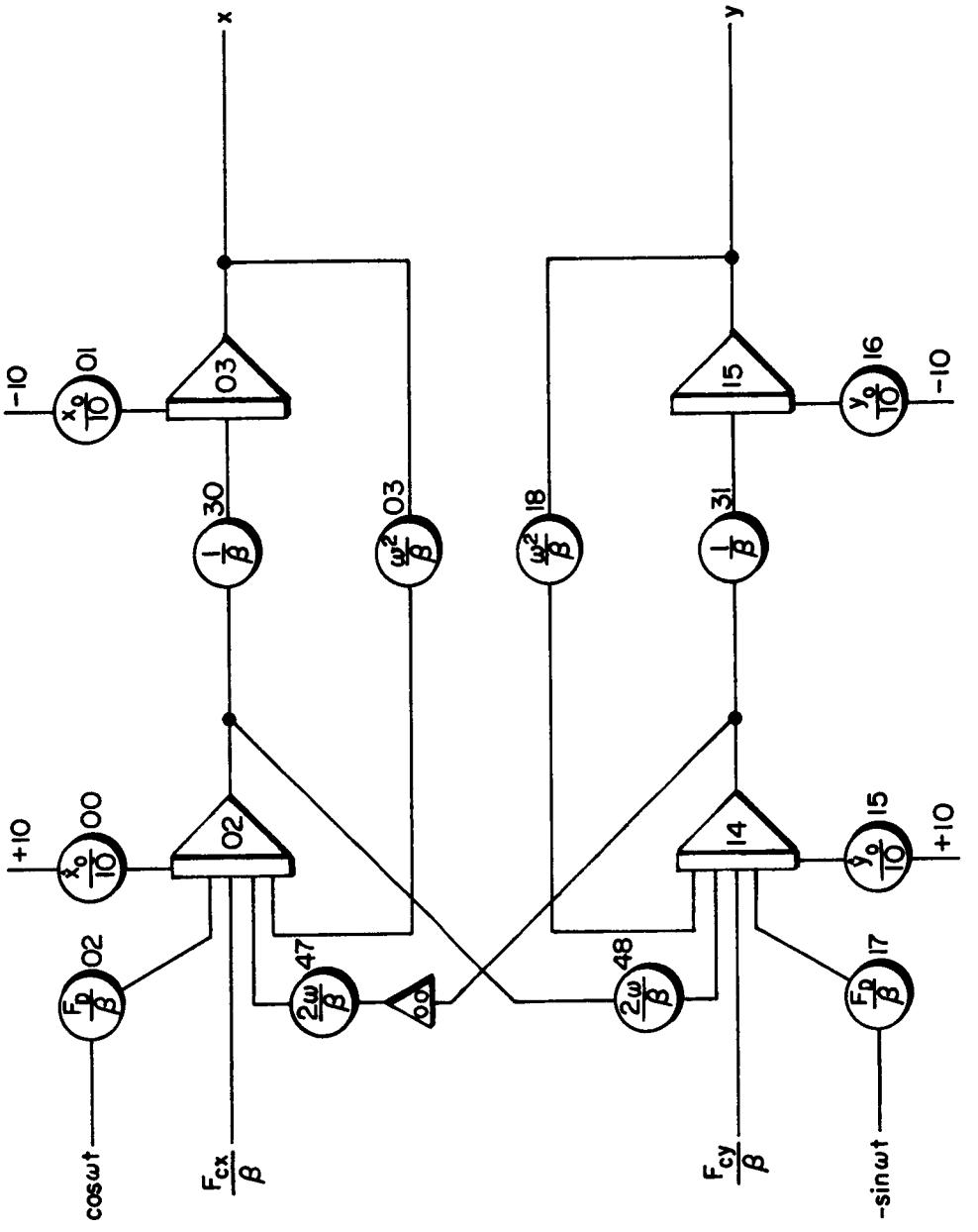

Fig. A-3. Vehicle Dynamics (TR-48 #2)

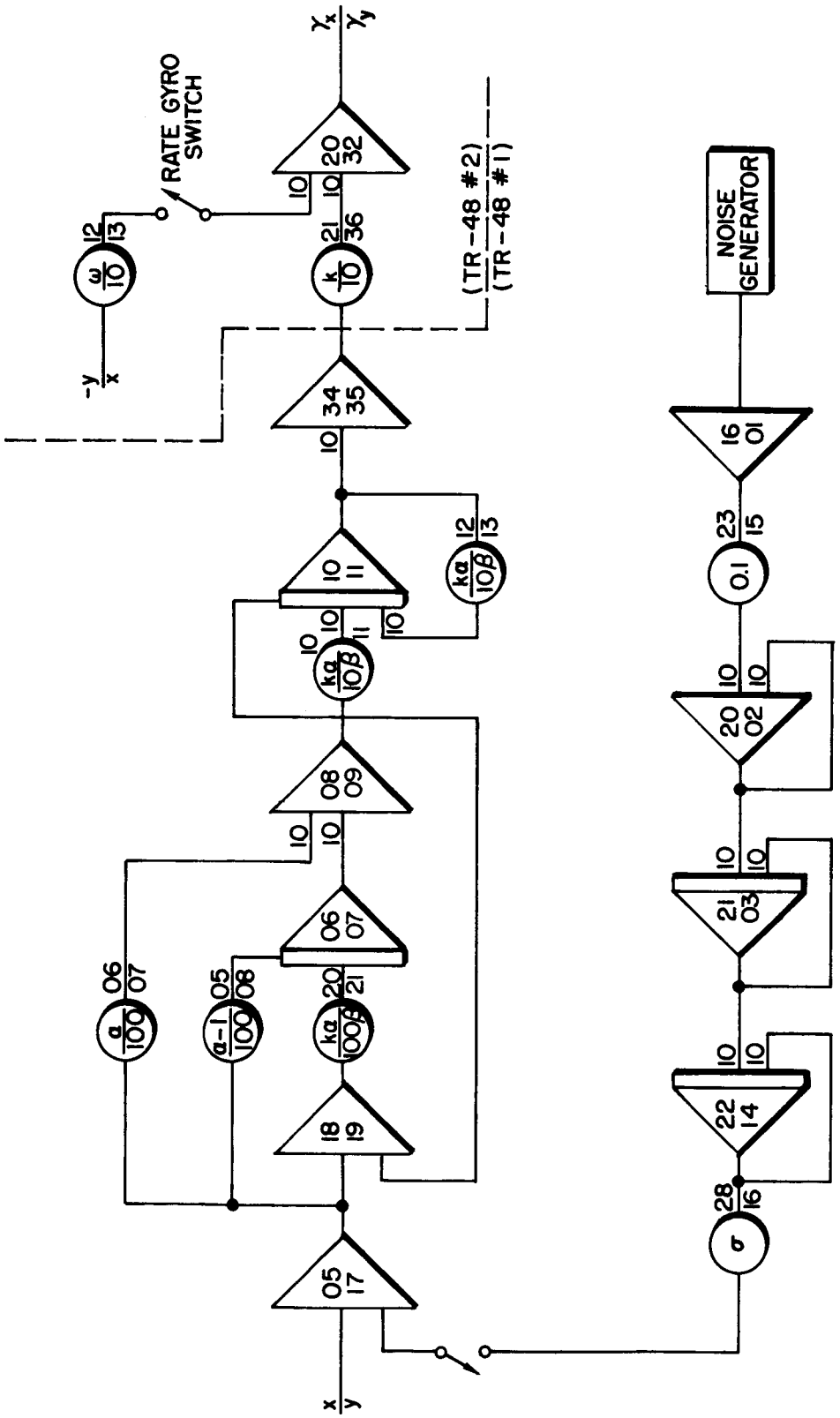

Fig. A-4. Filter For On-Off Control

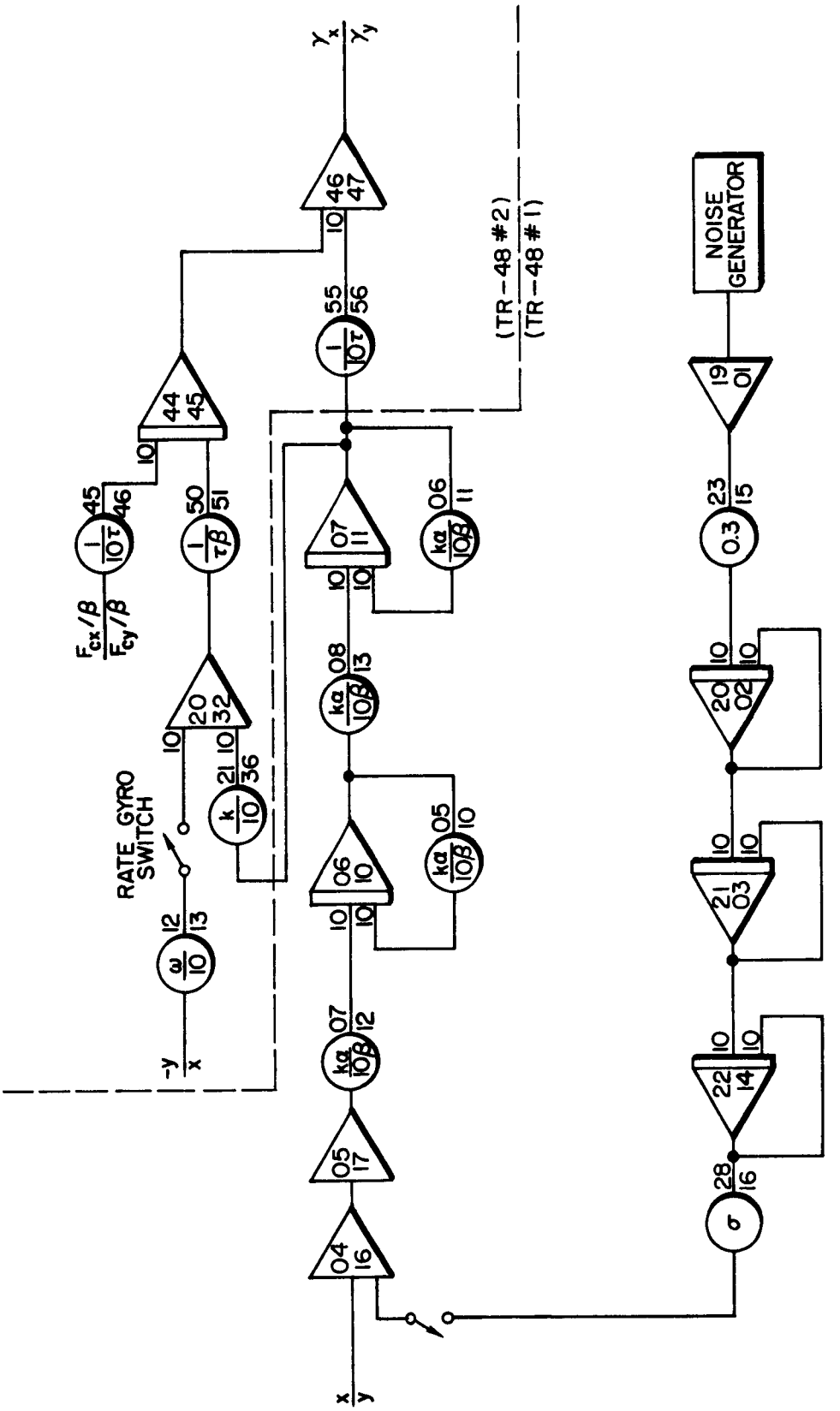

Fig. A-5. Filter For PWPF Control

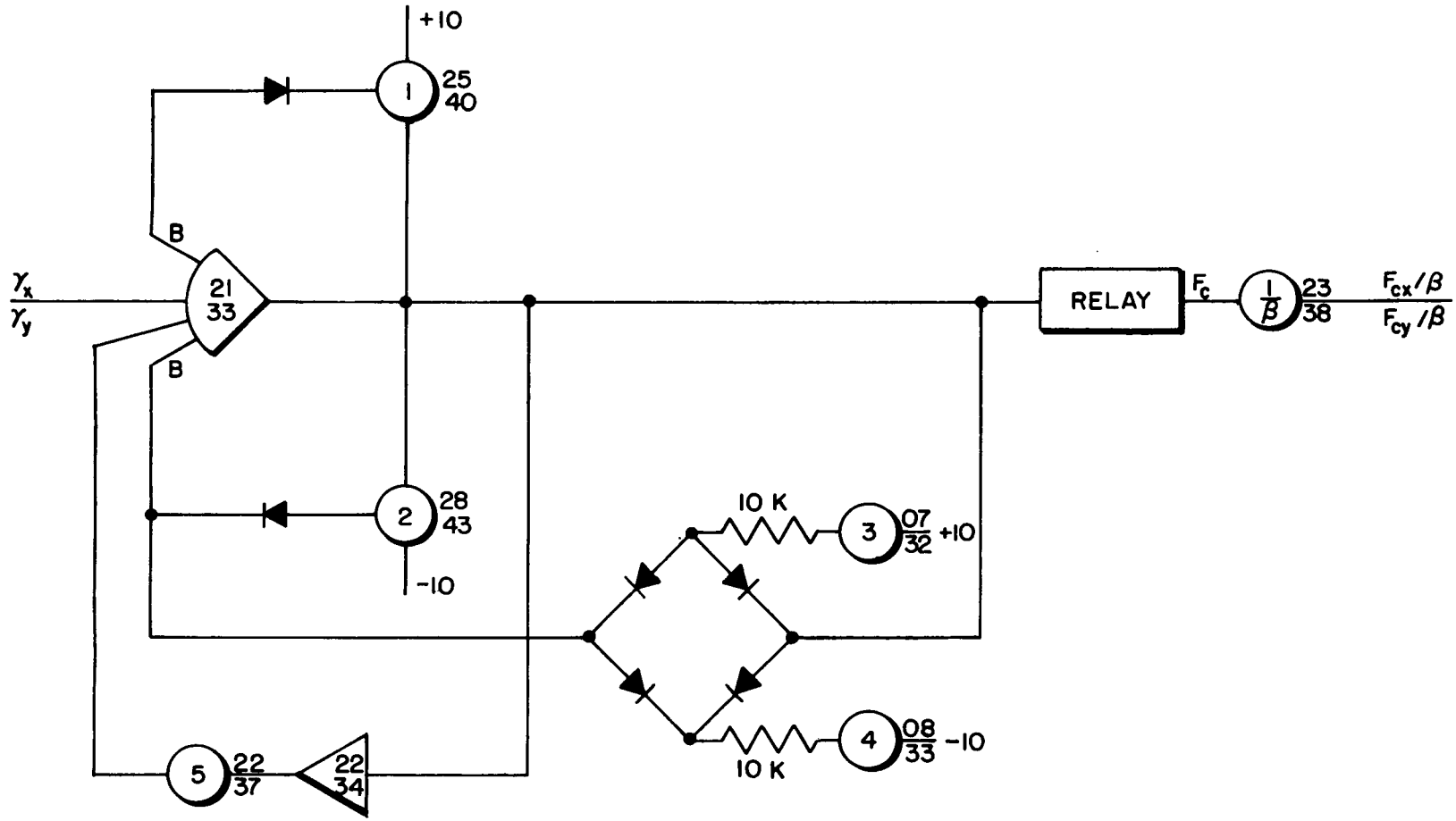

Fig. A-6. Discontinuous Control (TR-48 #2)

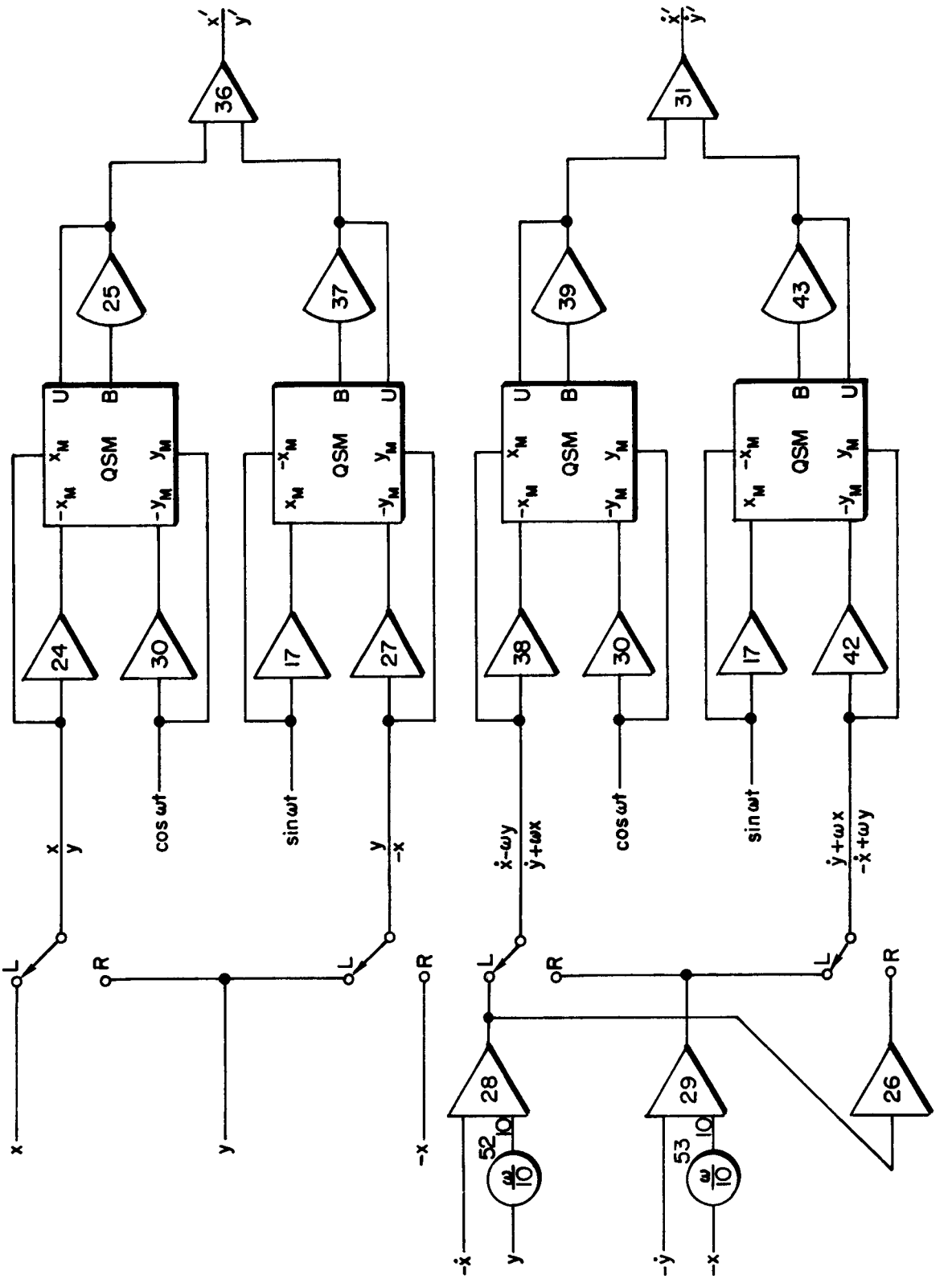

Fig. A-7. Coordinate Transformation (TR-48 #2)

00	01	02	03	04
0.490 05 $(\alpha-1)/100$	0.500 06 $\alpha/100$	0.500 07 $\alpha/100$	0.490 08 $(\alpha-1)/100$	09
0.500 10 $k\alpha/10\beta$	0.500 11 $k\alpha/10\beta$	0.500 12 $k\alpha/10\beta$	0.500 13 $k\alpha/10\beta$	14
0.100 15 Noise Level	0.146 16 Noise Level	17	18	19
0.050 20 $k\alpha/100\beta$	0.050 21 $k\alpha/100\beta$	22	0.100 23 Noise Level	24
25	26	27	0.150 28 Noise Level	29
30	31	32	33	34
35	36	37	38	39
40	41	42	43	44
45	46	47	48	49
50	51	52	53	54
55	56	57	58	59

Pot-Set List For On-Off Control (TR-48#1)

00	01	02	03	04
0.500 05 kα/10β	0.500 06 kα/10β	0.500 07 kα/10β	0.500 08 kα/10β	09
0.500 10 kα/10β	0.500 11 kα/10β	0.500 12 kα/10β	0.500 13 kα/10β	14
0.300 15 Noise Level	0.780 16 Noise Level	17	18	19
20	21	22	0.300 23 Noise Level	24
25	26	27	0.800 28 Noise Level	29
30	31	32	33	34
35	36	37	38	39
40	41	42	43	44
45	46	47	48	49
50	51	52	53	54
55	56	57	58	59

Pot-Set List For PWPF Control (TR-48#1)

0.100 00 $\dot{x}(0)/10$	0.100 01 $x(0)/10$	0.100 02 F_D/β	0.100 03 ω^2/β	04
05	0.100 06 $1/\beta$	0.096 07 Deadzone	0.100 08 Deadzone	09
10	0.100 11 $1/\beta$	0.100 12 $\omega/10$	0.100 13 $\omega/10$	14
0.000 15 $\dot{y}(0)/10$	0.000 16 $y(0)/10$	0.036 17 F_D/β	0.100 18 ω^2/β	19
20	0.100 21 k/10	0.400 22 Hysteresis	0.100 23 $1/\beta$	24
0.770 25 Limiter	26	27	0.667 28 Limiter	29
0.100 30 $1/\beta$	0.100 31 $1/\beta$	0.096 32 Deadzone	0.099 33 Deadzone	34
35	0.100 36 k/10	0.400 37 Hysteresis	0.100 38 $1/\beta$	39
0.768 40 Limiter	41	42	0.091 43 Limiter	44
0.133 45 1/10T	0.133 46 1/10T	0.200 47 $2\omega/\beta$	0.200 48 $2\omega/\beta$	49
0.133 50 $1/T\beta$	0.133 51 $1/T\beta$	0.100 52 $\omega/10$	0.100 53 $\omega/10$	54
0.133 55 1/10T	0.133 56 1/10T	57	58	59

Pot-Set List For Both Controls (TR-48#2)
(Pots 45,46,50,51,55,56 For PWPF Control Only)